



**NTNU – Trondheim**  
Norwegian University of  
Science and Technology

# Shear Properties of Nordic Glulam CE L40c

**Line Sigbjørnsen**

Civil and Environmental Engineering

Submission date: June 2012

Supervisor: Kjell A Malo, KT

Norwegian University of Science and Technology  
Department of Structural Engineering



**Department of Structural Engineering**

Faculty of Engineering Science and Technology

**NTNU- Norwegian University of Science and Technology**

ACCESSIBILITY

OPEN

## MASTER THESIS 2012

SUBJECT AREA: CONSTRUCTION	DATE: 10.06.2012	NO. OF PAGES: 88
TITLE:  <b>Shear Properties of Nordic Glulam CE L40c</b>  Skjæregenskaper til Nordisk Limtre CE L40c		
BY:  LINE SIGBJØRNSEN		
<p><b>SUMMARY:</b> The aims of this report are to investigate whether a new specimen is suitable for shear testing and to investigate the shear properties of Nordic glulam CE L40c. A total number of 56 shear tests were carried out. The specimens were modelled numerically and tested in the laboratory using video extensometry to measure surface strains. Approximately 40 % of all specimens produced a nice shear surface at failure. Practically all specimens formed two vertical cracks along the sides of the shear plane. These cracks had their origin from areas along the cuts where concentrations of tension perpendicular to grain were observed in results from numerical analysis and laboratory testing. The characteristic shear strength of CE L40c, <math>f_{v,g,k}</math>, was estimated between 2.6 MPa and 3.6 MPa, depending on specimen size. The average 5-percentile of the stiffness, <math>G_{g,05}</math>, was estimated approximately 970 MPa.</p>		
RESPONSIBLE TEACHER: KJELL ARNE MALO		
SUPERVISOR(S): KJELL ARNE MALO, PÅL ELLINGSBØ		
CARRIED OUT AT: DEPARTMENT OF STRUCTURAL ENGINEERING		



## **Preface**

This master thesis was written during spring 2012 at the Norwegian University of Science and Technology (NTNU) at the Department of Structural Engineering, Faculty of Engineering, Science and Technology NTNU.

I would like to thank my supervisor; Professor Kjell Arne Malo, who has given me guidance and support during this period. I would also like to thank PhD student Pål Ellingsbø for support on ARAMIS, ABAQUS and other obstacles I have met. I am also grateful to laboratory workers Gøran Loraas and Terje Petersen for cutting the specimens and assisting me in the laboratory. Finally, I would like to thank fellow student Torgrim Østen for proofreading.

Trondheim 10.06.2012

Line Sigbjørnsen



## **Abstract**

The aims of this report were to investigate whether a new specimen is suitable for shear testing and to investigate the shear properties of Nordic glulam CE L40c.

A total number of 56 shear tests were carried out; the results from 43 of these tests were further investigated by means of probability calculations regarding shear strength and 41 regarding shear stiffness.

The specimens were modelled numerically and tested in the laboratory using video extensometry to measure surface strains. The results from the numerical modelling showed an even distribution of shear stress along the height of the shear plane, but also areas of tension perpendicular to fibres were observed. These areas appeared along the cuts, close to the area of interest. The results from the laboratory testing were found to correspond well to the numerical results.

Approximately 40 % of all specimens split in half and produced a shear surface at failure, while the remaining 60 % did not split in half. Practically all specimens formed two vertical cracks along the sides of the shear plane. These cracks had their origin from areas along the cuts where concentrations of tension perpendicular to grain were observed. The specimen needs further optimization, which requires further investigation.

The characteristic shear strength of CE L40c,  $f_{v,g,k}$ , was estimated between 2.6 MPa and 3.6 MPa, depending on specimen size. This corresponds well to values found in literature. Nevertheless, it is suspected that these values might be underestimated due to tension perpendicular to fibres close to the shear area, which may result in improper shear failure. The average 5-percentile of the stiffness,  $G_{g,05}$ , was estimated approximately 970 MPa. This is relative high compared to values from literature; which might be due to a simplified estimation method for the G-modulus in this research. A closer look into the G-modulus is recommended.



## Sammendrag

Formålet med denne rapporten er å finne ut om et nytt prøvestykke egner seg til skjærtesting, og også utforske skjæregenskapene til Nordisk limtre CE L40c.

Totalt ble det gjennomført 56 skjærtester. Resultatene fra 43 av disse testene ble tatt med i sannsynlighetsberegninger som gjelder skjærstyrke, mens resultatene fra 41 av testene ble tatt med i sannsynlighetsberegninger som gjelder skjærstivhet.

Prøvestykkene ble modellert numerisk, og deretter testet i laboratoriet med videomåling av overflatetøyninger. Resultatene fra de numeriske modelleringene viste en jevn fordeling av skjærspenning over høyden av skjærplanet, men også områder med strekk normalt på fiberretning ble observert. Disse områdene oppstod langs utskjæringene, nær skjærområdet. Resultatene fra laboratoriet stemte godt overens med resultatene fra den numeriske modelleringen.

Omtrent 40 % av alle prøvestykkene delte seg i to og dannet et skjærplan. De resterende 60 % av prøvestykkene delte seg ikke i to. Så å si alle prøvestykkene fikk to vertikale sprekker langs sidene av skjærplanet. Disse sprekke hadde opphav fra områdene langs utskjæringene hvor konsentrasjonen av strekk normalt på fiberretning ble observert. Videre optimalisering av prøvestykket er anbefalt.

Den karakteristiske skjærstyrken til CE L40c,  $f_{v,g,k}$ , ble estimert til mellom 2,6 MPa og 3,6 MPa, avhengig av størrelsen på prøvestykkene. Dette korresponderer bra med verdier fra litteraturen. Likevel er det mistanke om at disse verdiene kan være underestimert på grunn av strekk normalt på fiberretning i områder nær skjærplanet, noe som kan resultere i at bruddet ikke er et rent skjærbrudd. Gjennomsnittet av 5-prosentilen til stivheten,  $G_{0,05}$ , ble estimert til omtrent 970 MPa. Dette er et relativt høyt tall sammenlignet med verdier fra litteraturen; noe som kan ha årsak i at en forenklet estimeringsmetode for G-modulen ble brukt i denne rapporten. Det er anbefalt å se nærmere på G-modulen.



## Contents

Abstract .....	III
Sammendrag .....	V
Introduction.....	1
Symbols .....	1
Main symbols .....	1
Subscripts .....	2
Review of literature.....	3
Method.....	9
Density and moisture content.....	11
Numerical modelling .....	12
Part one .....	15
Numerical modelling .....	15
Results of modelling .....	18
Laboratory testing .....	21
Results of testing .....	21
Discussion .....	23
Part two .....	25
Numerical modelling .....	25
Results of modelling .....	27
Laboratory testing .....	28
Results of testing .....	28
Discussion .....	34
Part three .....	39
Numerical modelling .....	39
Results of modelling .....	40
Laboratory testing .....	42
Results of testing .....	42
Discussion .....	43
Results from part two and three merged .....	45
Discussion .....	48
Conclusion and further work.....	51

References.....	53
Appendix A: Transformation from engineering constants to stiffness parameters, C.....	55
Appendix B: Results on time, extension and applied force from test machine INSTRON.....	59
Part one .....	59
Part two .....	61
Part three .....	63
Appendix C: Pictures of specimens after failure .....	65
Part one .....	65
Part two .....	66
Part three .....	68
Appendix D: Calculations concerning shear strength from INSTRON test machine and G- modulus from ARAMIS (video extensometry) .....	69
PART ONE .....	69
PART TWO .....	70
PART THREE .....	73

## Introduction

During this research, an answer to the following two questions will hopefully be found:

- A new type of specimen for testing of shear properties of wood is developed and examined in this research. How effective will this specimen be for shear testing?
- What are the shear properties of Nordic glulam CE L40c?

Professor at the department of structural engineering at NTNU, Kjell Arne Malo who developed the idea behind this new specimen was inspired by cruceform test specimens used for bi-axial testing of different materials. The specimen will first be modelled numerically to get an initial estimate on how it will behave during loading. Then, the specimens will be made and taken to the laboratory for shear testing. The testing will be monitored by cameras, saving a series of pictures to a computer to be used to obtain strains on the specimen surface during testing. Hopefully the results from the numerical models will fit the results from the laboratory testing. The specimens might need to be optimized several times before the optimal design is found.

The results of shear strength and stiffness from the laboratory testing will be analysed in order to estimate the shear properties of Nordic glulam CE L40c.

***This research is divided into three parts. A part consists of***

- 1. Numerical modelling of specimens in ABAQUS***
- 2. Testing the specimens in the laboratory***
- 3. Evaluation of the results from numerical modelling and testing***
- 4. Discussion; improving the specimens before the next part***

## Symbols

The symbols used in this report are listed below.

### Main symbols

- $H$  total height of specimen, in millimetres;
- $D$  depth of specimen, in millimetres;
- $W$  width of specimen, in millimetres;
- $h$  height of specimen shear plane, in millimetres;
- $t$  thickness of cuts of specimen, in millimetres;
- $l$  length of solid wood above cut of specimen, in millimetres;
- $A_{shear}$  cross-sectional area of shear plane, in square millimetres;

$F_{max}$	Maximum load (failure load), in newtons;
$f$	strength, in newtons per square millimetre;
$E$	modulus of elasticity, in newtons per square millimetre;
$G$	shear modulus, in newtons per square millimetres;
$\sigma$	stress;
$s$	standard deviation;

### **Subscripts**

$L$	longitudinal (in the direction of fibres);
$R$	radial direction of annual rings;
$T$	tangential direction of annual rings;
$X$	global horizontal direction in plane (width of specimen);
$Y$	global vertical direction in plane (height of specimen);
$Z$	global direction out of plane (depth of specimen);
$g$	Properties of glued laminated timber;
$k$	characteristic;
$l$	properties of laminations;
$m$	bending;
$t$	tension;
$v$	shear;
0	parallel to fibres;
90	perpendicular to fibres;
05	5-percentile;
<i>mean</i>	mean value;
<i>est</i>	estimated value;

## Review of literature

Several attempts on determining shear strength of wood have been carried out using different specimens and setups. Still, there is no applicable computation method for shear bearing capacity. However, the shear properties of wood have mainly been based on the notched shear block test (Dahl and Malo, 2009a). This test consists of a longitudinal oriented block which has two notched corners, forming two blocks. The smallest block rests on a fixed surface and is sheared off by applying a force on the largest block, as shown in figure 1.

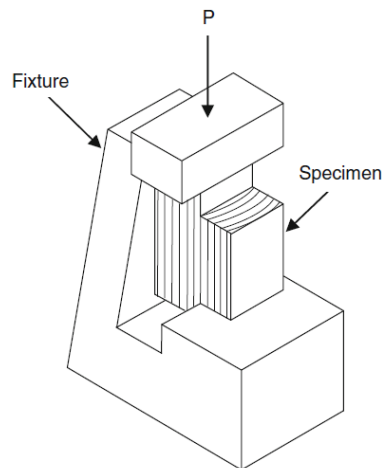


**Figure 1: Notched shear block test**

When investigating shear strength of wood, a pure shear plane with evenly distributed shear force is desired, but very difficult to obtain. There will always be an eccentricity that causes bending moments, which produces normal forces on the shear plane. When this happens, the results from such a test do not show the pure shear strength of wood, but a combination of shear strength and tensile or compressive strength. Also, an even distribution of shear and normal stresses along the failure surface is difficult to obtain. The notched shear block test has been criticized due to this error because the loading is eccentric and causes normal stresses on the shear plane (Dahl and Malo, 2009a).

A method for measuring the shear modulus parallel to fibres is presented in NS-EN 408 (2003) where a piece of wood is glued between two steel plates which is moved relative to each other so that the test piece experience shear as shown in figure 2. This method was investigated by Denzler and Glos (2007) to see whether the test results match the values for shear strength given in EN 338 and EN 384. They found that their test results did not confirm an increase in shear strength with increasing density as given in EN 338. This conclusion was also confirmed by Schickhofer (2001).

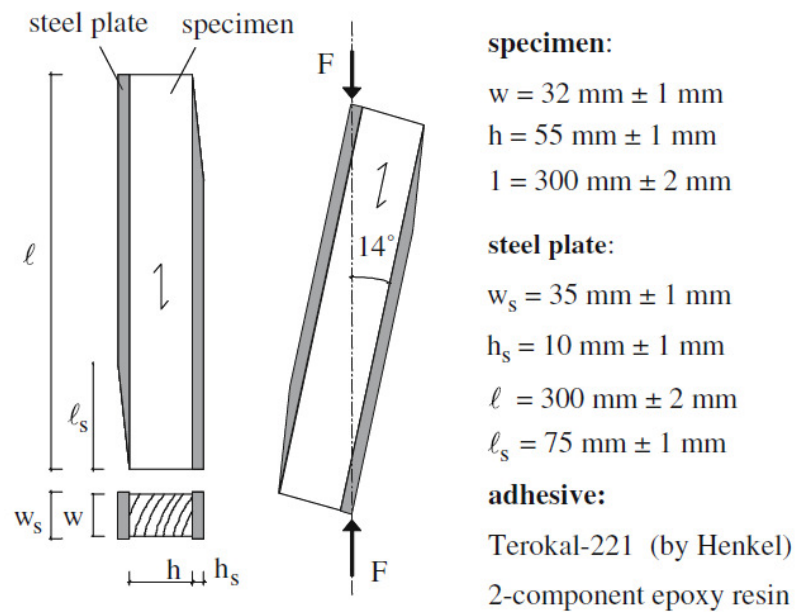


**Figure 2: Shear test according to EN 408**

Another test setup for determining shear moduli for wood is the Iosipescu shear test. This test has proven to give sufficient shear moduli for wood. It consists of a rectangular piece of wood with a notch at upper and lower middle of the piece (Dahl and Malo, 2009a). The piece is attached to a fixture, which allows the two loads to be applied such that the bending moment is zero, but the shear forces are nonzero over the critical section of the specimen as shown in figure 3.

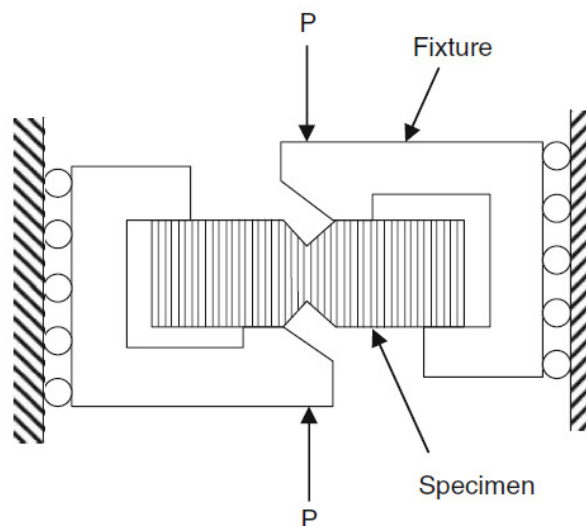


**Figure 3: The Iosipescu shear test**

All shear types of an orthotropic material can be tested by orienting the specimen within the material. However, even if the Iosipescu shear test gives a good approximation to the shear moduli of wood, the shear failure stress is less accurate due to improper failure of the

specimen. This is due to bending moment other places than in the critical shear section. Particularly radial or tangential oriented specimens, which have low tensile capacities in these directions, are vulnerable to improper failure.

Dahl and Malo (2009a, 2009b) use the Arcan shear test to investigate linear and nonlinear orthotropic shear properties of Norway spruce. This test pursues the idea of the Iosipescu test, but with a different fixture as shown in figure 4. The specimen is butterfly-shaped and the fixture allows the loading to be nicely distributed to the intended shear area.

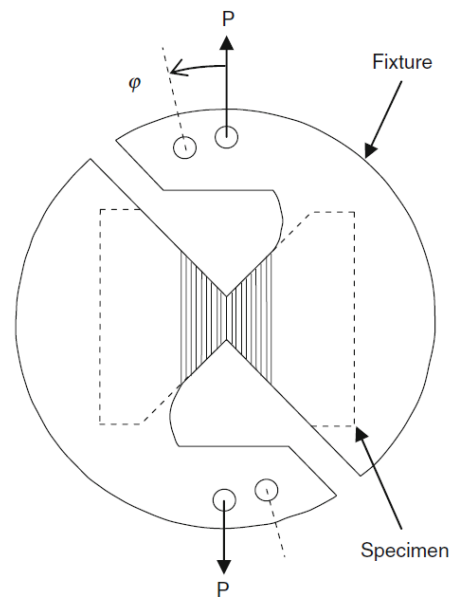


**Figure 4: The Arcan shear test**

By varying the angle  $\phi$  for the Arcan shear test, a combination of shear and normal stresses can be investigated. The specimen can be glued or bolted to the fixture. Finite element analysis and photo-elastic results have shown that the shear is approximately uniform over the critical section; hence, this test is considered the best choice by Dahl and Malo (2009a, 2009b) in their investigation. Their research concludes that the shear modulus and parameters describing nonlinear properties of clear softwood of Norway spruce found in the research corresponded well with similar values reported in literature. In figure 5, their calculated shear modulus is plotted together with values found in literature. The shear modulus were found for three configurations;  $G_{LR}$ ,  $G_{LT}$  and  $G_{RT}$  (rolling shear). However, the plastic parameters were found to often correlate with the initial shear moduli, but not so often with density. Also, the shear modulus did not correlate much with density. These conclusions are confirmed by Denzler and Glos (2007).

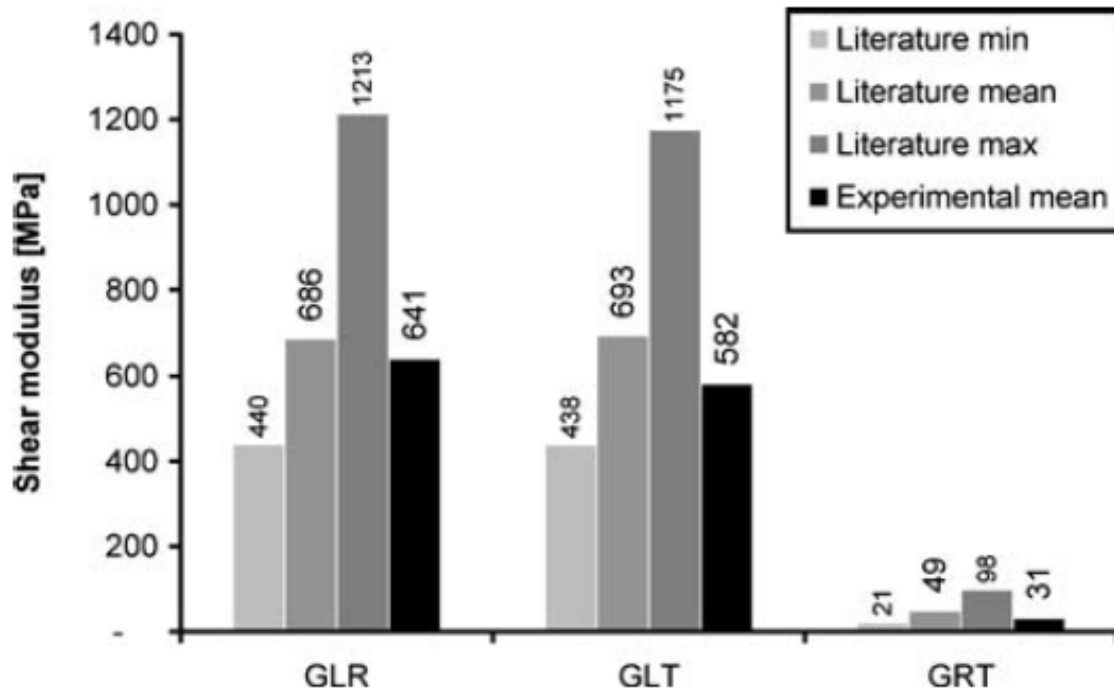


**Figure 5: Shear moduli found by Dahl and Malo (2009a) compared to literature min, literature mean and literature max (Dahl & Malo, 2009a)**

In NS-EN 338 (2003), structural timber of higher strength classes is given higher shear strength- and stiffness values. As a contrast, the German standard DIN 1052 uses a constant value of 3.5 MPa as shear strength of glulam (Klapp and Brüninghoff, 2005). The argumentation for a constant value is that so far, no relationship between higher strength classes and higher shear strength is established.

NS-EN 338 (2003), is based on equations found in NS-EN 384 (2004), which states that the shear modulus can be calculated as 6.25 % of the longitudinal modulus of elasticity

$$G_{mean} = \frac{E_{0,mean}}{16}$$

In the European Standard EN 1194 (1999), the shear strength of glulam is a function of lamina tensile strength

$$f_{v,g,k} = 0.32(f_{t,0,l,k})^{0.8}$$

According to Schickhofer (2001), this correlation between shear strength and tensile strength of the lamina cannot be confirmed. A draft of the new standard NS-EN 14080 (2011) has been submitted for formal vote adoption. This standard replaces NS-EN 1194 (1999). According to NS-EN 14080 (2011), the shear strength and -stiffness of glulam have constant values for all strength classes as shown in table 1.

**Table 1: Shear strength and stiffness properties of combined glulam according to NS-EN 14080 (20011) in MPa**

<b>Shear strength (shear and torsion)</b>	$f_{v,g,k}$	<b>3,5</b>
<b>Rolling shear strength</b>	$f_{r,g,k}$	<b>1,2</b>
<b>Shear modulus</b>	$G_{g,mean}$	<b>650</b>
	$G_{g,05}$	<b>542</b>
<b>Rolling shear modulus</b>	$G_{r,g,mean}$	<b>65</b>
	$G_{r,g,05}$	<b>54</b>

Klapp and Brüninghoff (2005) found that there is a size-effect (volume effect) on shear capacity of timber, which means that larger beams have a lower shear bearing capacity than smaller beams.



## Method

The new specimen investigated in this report pursues the basic idea behind the Iosipescu and Arcan shear tests; loading without eccentricity, but without any fixtures. It is a simple composition consisting of one rectangular piece of wood which is cut to the middle from two sides, one upper cut and one lower cut, forming a vertical shear plane in the middle of the piece, see figure 6. The cuts have an inclination of 45 degrees.

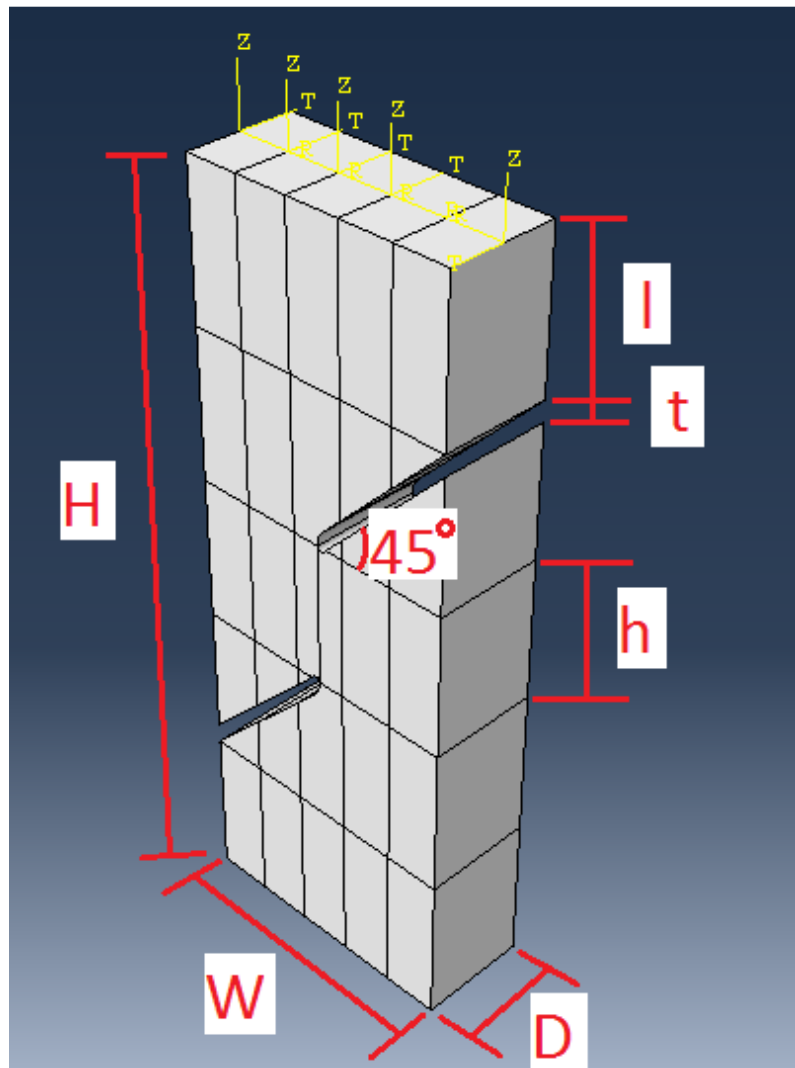


**Figure 6: Specimen used for investigation of shear properties: H is the total height, W is the width, D is the depth, h is the height of the shear plane, t is the thickness of the cut and l is the length of wood continuing above (or below) the cut.**

The dimensions H, W, D, h, t, and l must be determined to get optimal properties of the specimen; which means that an even distribution of shear over the shear plane is desired, without influence of any other forces; particularly not tension perpendicular to fibres, as wood is very weak in this direction.

No fixture is needed on the specimen; compression is applied directly on top of it as shown in figure 7. By removing a piece of the specimen, the shear plane emerges, see figure 8.

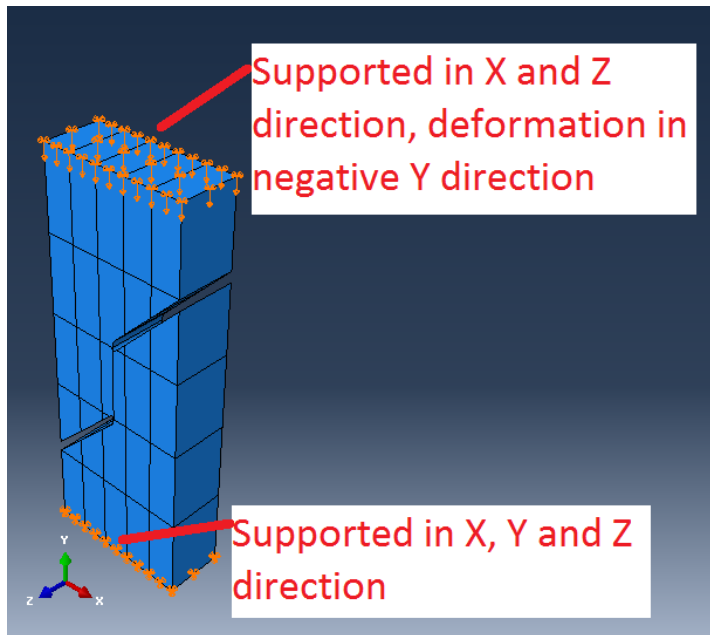


**Figure 7: Support and load application**

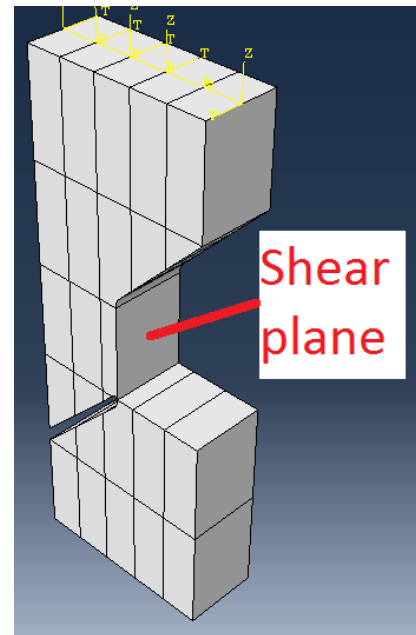


**Figure 8: Shear plane**

The specimen was modelled using the numerical software ABAQUS and then tested in the laboratory.

Video extensometry was used during testing to measure strains on the surface of the specimen; two cameras were focused on the area of interest (the area between the cuts) and approximately ten pictures per second were saved to the computer. The surface of which the pictures were taken must be properly lighted; two spotlights were focused on the specimen. The computer program ARAMIS was used to calculate strains on the surface of the specimens. This program recognize black dots on a white surface and measure how much these dots move relative to each other from the first picture to the current picture. Hence, on the specimens, the area of interest was sprayed white with small, black dots as shown in figure 9.

The glulam used for the specimens was kept in an acclimatized room with a relative humidity of  $(65 \pm 5) \%$  and a temperature of  $(20 \pm 2) ^\circ\text{C}$  as described in EN 380 (1993). The shear tests were carried out using a 100 kN INSTRON test machine stationed in the acclimatized room, see figure 10.

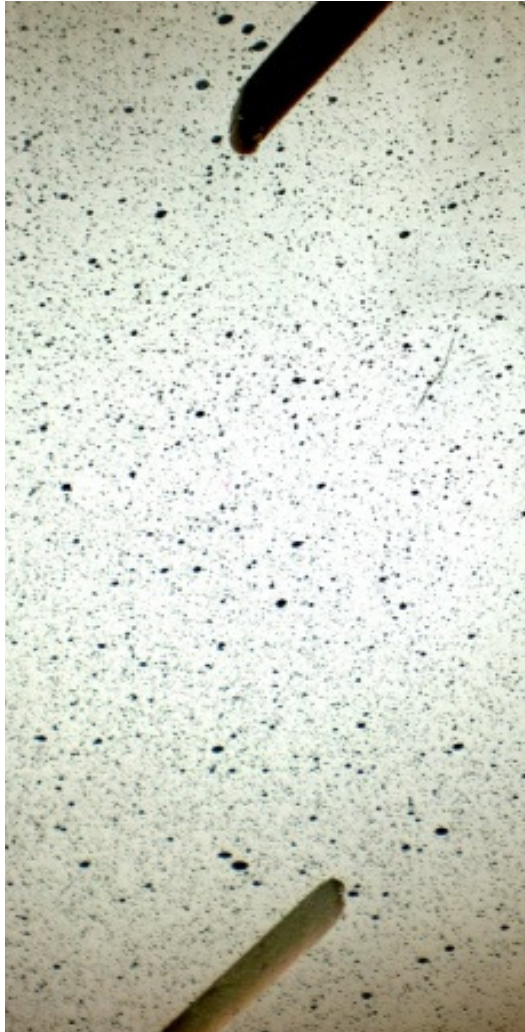


**Figure 9: Black dots on white background for video extensometry**



**Figure 10: Specimen in INSTRON test machine with cameras and spotlights on tripod fixed at the area of interest**

The glulam used in this investigation, CE L40c, is the standard glulam quality in Norway and corresponds to the strength of GL 32c (Moelven). CE L40c is made of 45 mm thick and 90 mm deep lamina of Norway spruce.

The shear strength measured is shear parallel to fibre direction; a combination of LR and LT configurations.

### **Density and moisture content**

After laboratory testing, the density and moisture content of the material was determined according to ISO 3130 (1975) and ISO 3131 (1975). Three prisms with square cross-section of 20 mm sides and length along the fibres of  $25 \pm 5$  mm were cut from each specimen after testing, using the material from the same lamina in which the shear failure occurred; above or below the shear plane. The prisms were measured and weighed before soaked in water for at least two days to obtain their saturated condition. Then, the prisms were measured and weighed again before they were dried to obtain their absolutely dry condition. The

drying takes place at a temperature of  $(103 \pm 2)$  °C for at least two days. Finally, the prisms were weighed and measured in their dry condition. The moisture content,  $W$ , of each prism was calculated by the formula:

$$W = \frac{m_1 - m_2}{m_2} * 100 \quad (1)$$

Where

$m_1$  is the mass, in grams, of the prism before drying (acclimatized condition), and

$m_2$  is the mass, in grams of the test piece in absolutely dry condition.

The density may be adjusted to a density at 12 % moisture content, and is calculated by the following formula:

$$\rho_{12} = \text{density estimated at 12 \% moisture content} = \rho_w \left[ 1 - \frac{(1 - K)(W - 12)}{100} \right] \quad (2)$$

where  $K$  is the coefficient of volumetric shrinkage for a change in moisture content of 1 % and may be taken as  $0.85E10^{-3}\rho_w$  for approximate calculations. The formula is valid for moisture content from 7 to 17 %.

And:

$$\rho_w = \text{density at moisture content } W = \frac{m_w}{V_w} \quad (3)$$

where  $m_w$  is the mass of the prism at moisture content  $W$ , and

$V_w$  is the volume of the prism at moisture content  $W$ .

### Numerical modelling

Only the linear behaviour is simulated in ABAQUS, using linear elastic material properties of Norway spruce with density  $400 \text{ kg/m}^3$  as shown in table 2.

**Table 2: Linear elastic stiffness properties of Norway spruce with density  $400 \text{ kg/m}^3$  used for modelling based on results from Dahl (2009).**

Symbol	$E_{LL}$	$E_{RR}$	$E_{TT}$	$\nu_{LR}$	$\nu_{LT}$	$\nu_{RT}$	$G_{LR}$	$G_{LT}$	$G_{TR}$
Value	10000 MPa	800 MPa	400 MPa	0.5	0.6	0.6	600 MPa	600 MPa	30 MPa

The specimens were modelled such that all the laminas of the laminate were oriented the same direction, except for one of the outward lamina, which was rotated 180 degrees relative to the others (seen from above). This is shown in figure 11.

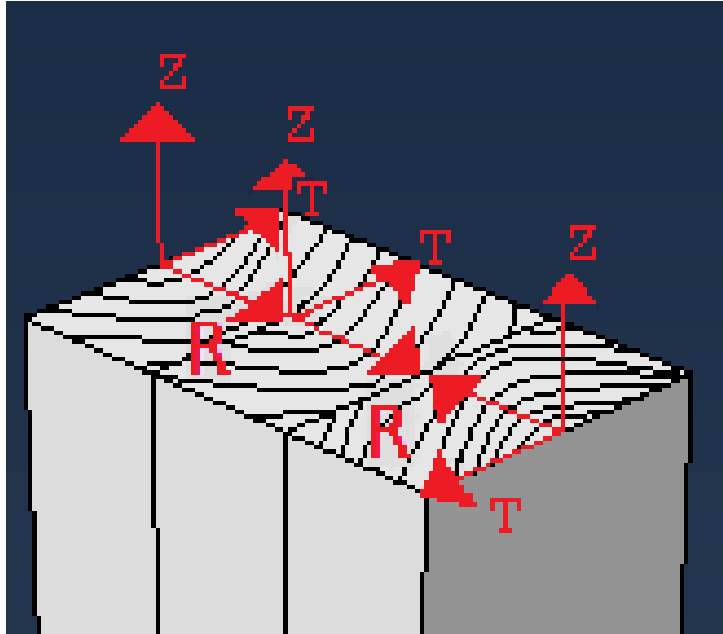


Figure 11: Orientation of annual rings.



## **Part one**

### **Numerical modelling**

First, to get an idea on how stresses distribute using different dimensions on specimens, a collection of nine specimens were modelled. The width of the specimen and the height of the shear plane was varied one at a time. For these nine specimens, a lamina thickness of 33 mm was used. The total widths of the specimens were 99 mm, 165 mm and 231 mm. All specimens were 600 mm high and 90 mm deep. The height of the shear planes were 65 mm, 115 mm and 165 mm, as shown in figure 12.

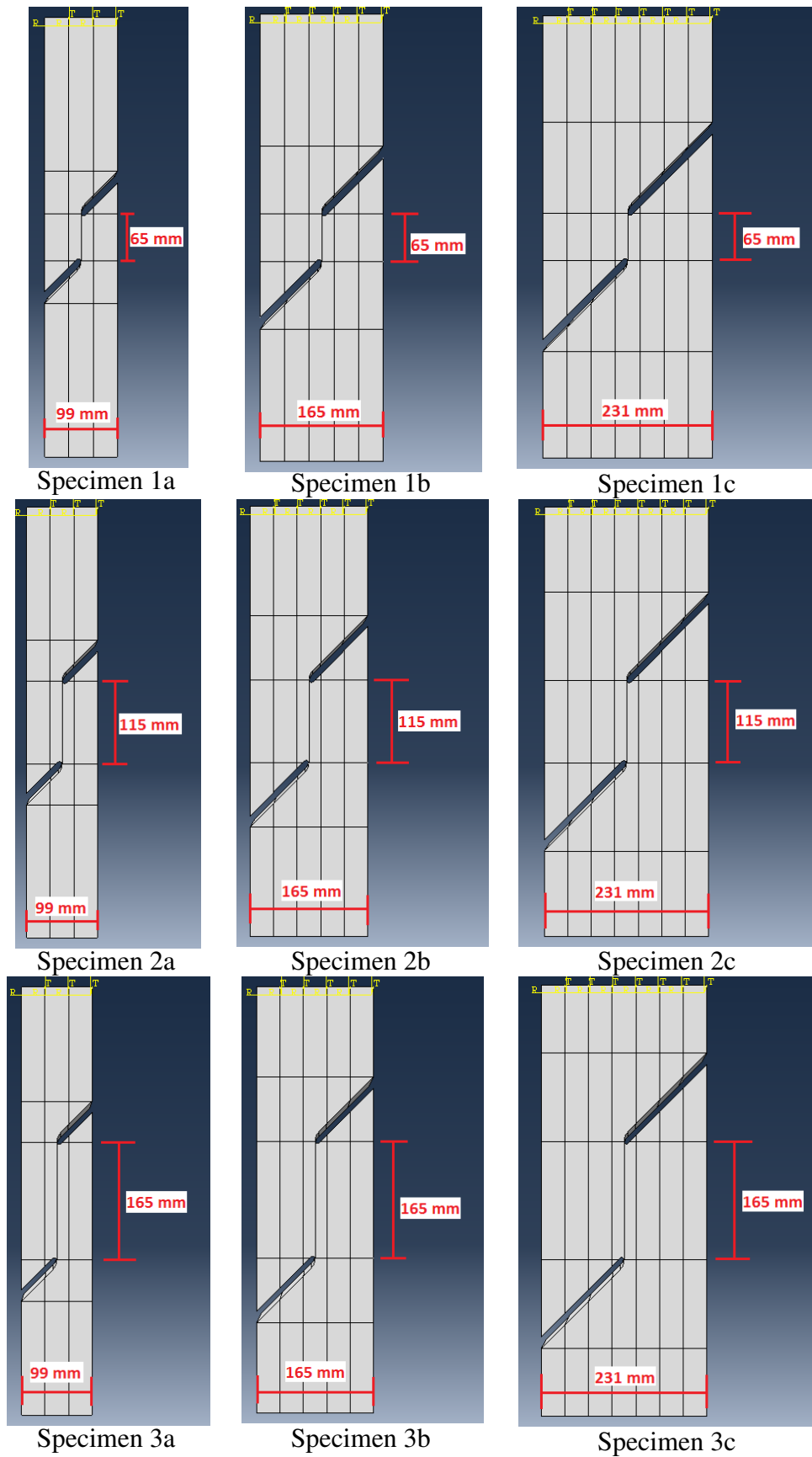


**Figure 12: The nine first specimens modelled in ABAQUS. All specimens have a total height of 600 mm and are 90 mm deep. The height of the shear plane and the width of the specimens vary as shown above.**

At first attempt, the specimens were modelled with sharp corners for the cuttings. This gave large local stresses, therefore, the edges where rounded. Still, there were large local stresses, so a finer mesh was applied just around the ends of the cuttings and also along the shear plane. This is shown in figure 13. Also, a remeshing rule was applied around the cuttings and along the shear plane as seen figure 14. The remeshing rule generates a new mesh whenever the elements of the old one are too deformed.

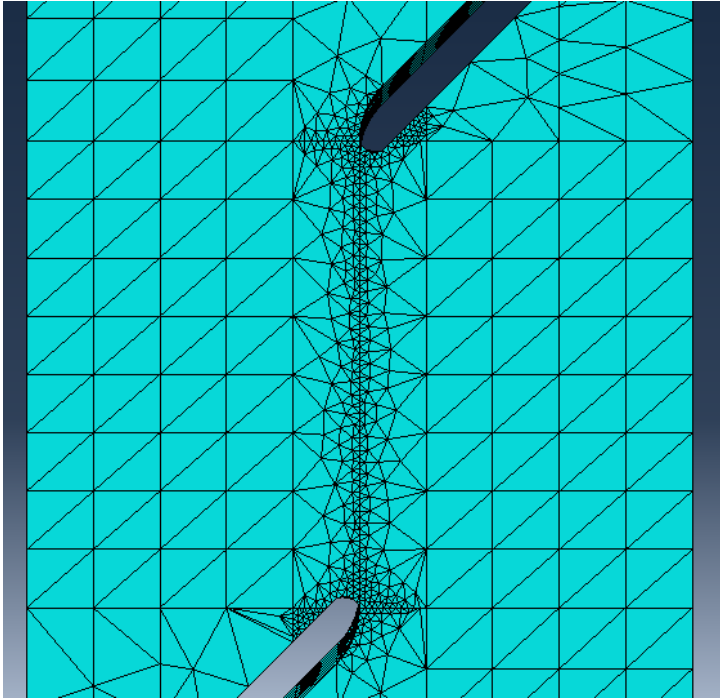


**Figure 13: A fine mesh is applied around the ends of the cuts and along the shear plane.**

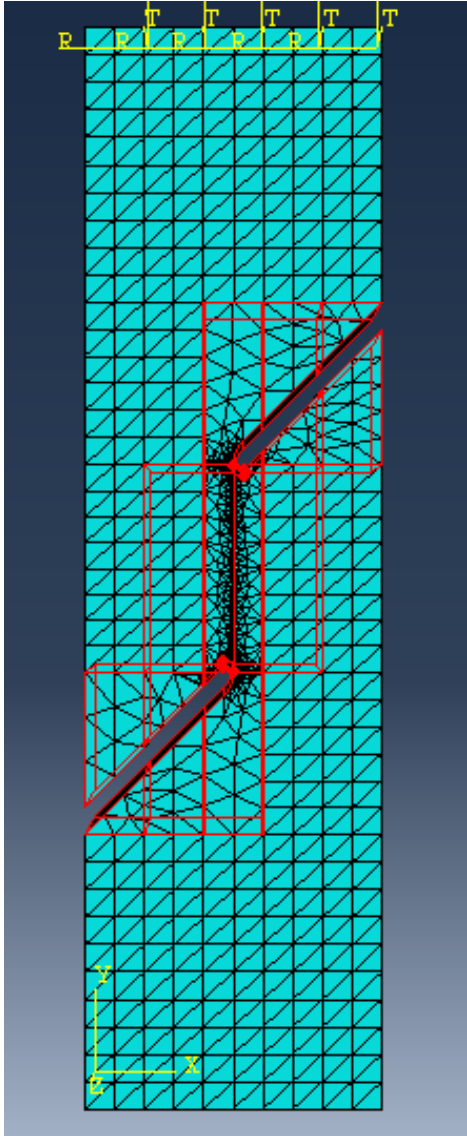


**Figure 14: The red boxes show the area where a remeshing rule is applied.**

The three specimens 1a, 2b, and 3c (diagonal) in figure 12 were chosen to be tested in the lab in order to investigate the behaviour when both width,  $W$ , and height of shear plane,  $h$ , were varied from specimen to specimen. These three specimens were modelled again in ABAQUS, now with a lamina thickness of 45 mm, as used for Norway spruce. The specimens were given names from their dimensions as shown in figure 15.

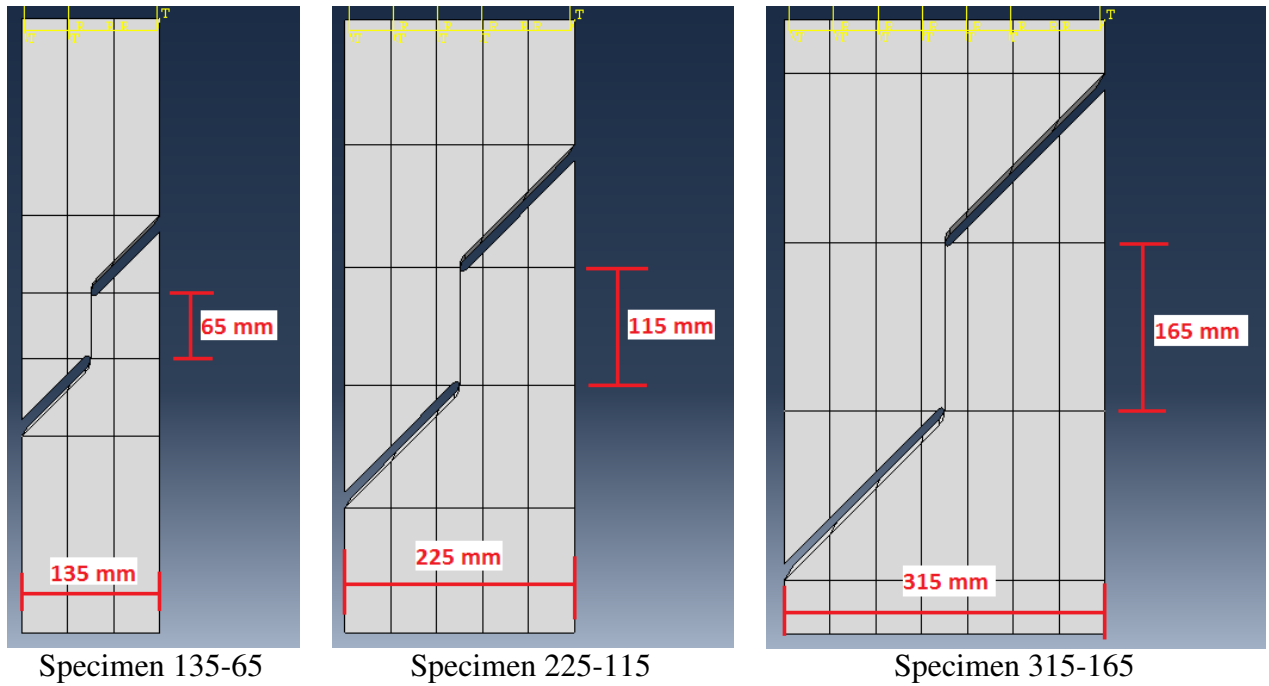


**Figure 15: Specimens 1a, 2b and 3c from figure 12 modelled in ABAQUS with lamina thickness 45 mm to be tested in the lab.**

The cuttings were 16 mm thick and were cut at an angle of 45° through the depth of the specimen. They touch the vertical imagined shear plane at their very outermost point in horizontal direction as shown in figure 16.

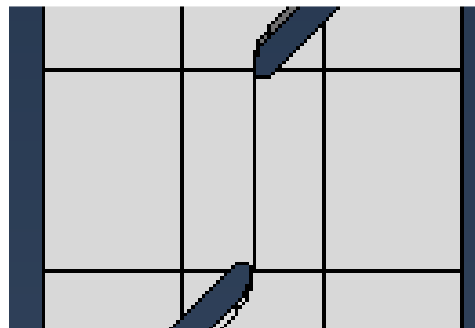


**Figure 16: The cuts touch the imagined shear plane at their outermost point in horizontal direction**

The models were loaded until  $\tau_{xy} \sim 10 \text{ MPa}$  on the shear plane in order to go beyond the limit of shear strength for wood. The loading in ABAQUS were governed by deformation in negative vertical direction on top of the specimen as shown in figure 7.

### Results of modelling

The contour plots of surface shear in global XY-direction from the first nine specimens modelled in ABAQUS are shown in figure 17.

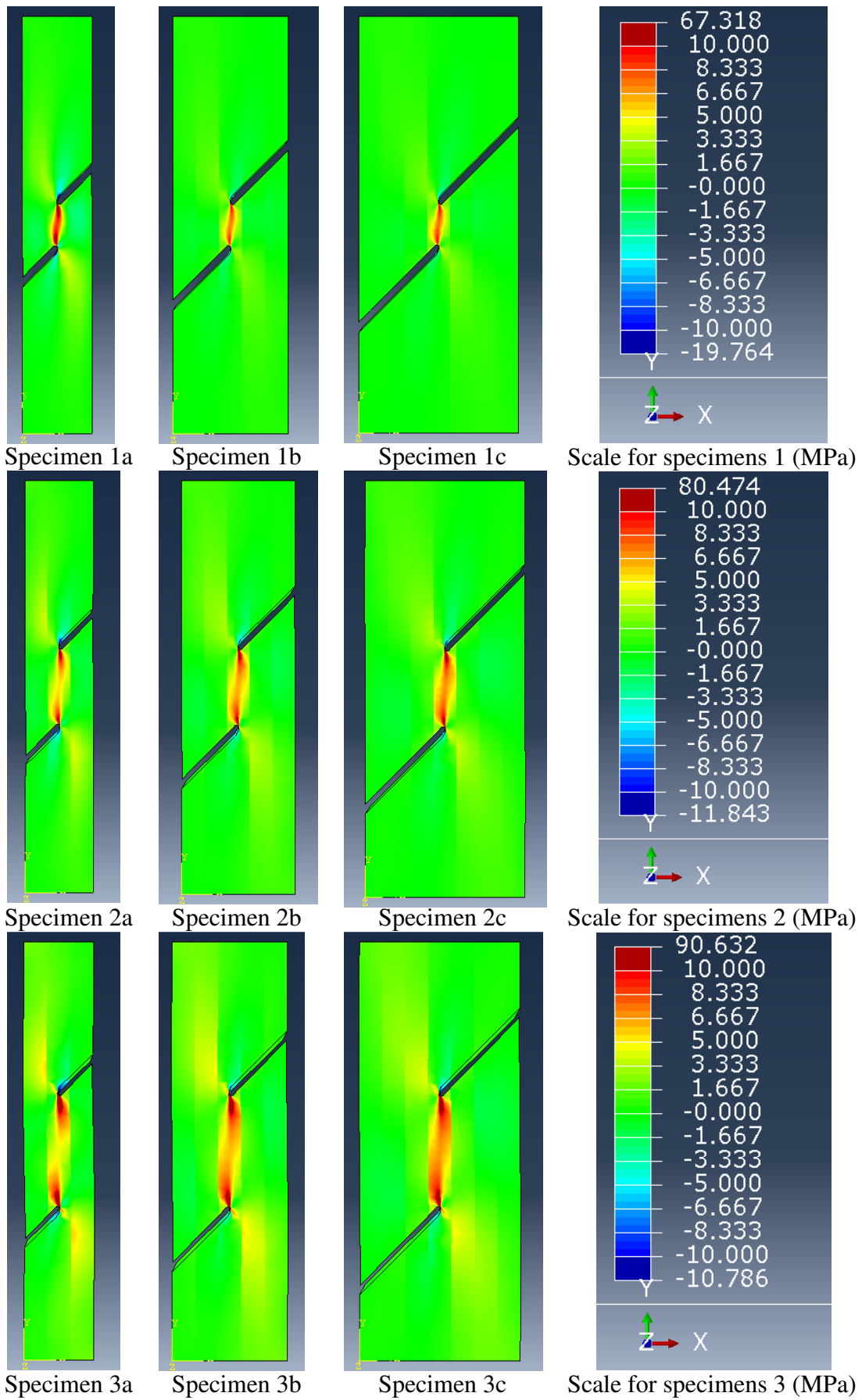


**Figure 17: Contour plots of surface shear  $\tau_{XY}$  for glulam of 33 mm lamina**

As seen from figure 17, the shear distribution along the height of the shear plane is slightly S-shaped. The shear intensity is approximately evenly distributed for the specimens in row one, but becomes more varied as the height of the shear plane increases.

The contour plots of surface shear in global XY-direction of specimens 1a, 2b and 3c from figure 12 are shown below in figure 18. The average shear stress over the height of the shear plane is approximately 10 MPa. The distribution of shear stress along the height of the shear plane is slightly S-shaped; the specimens with lower height of shear plane having a more even shear distribution.

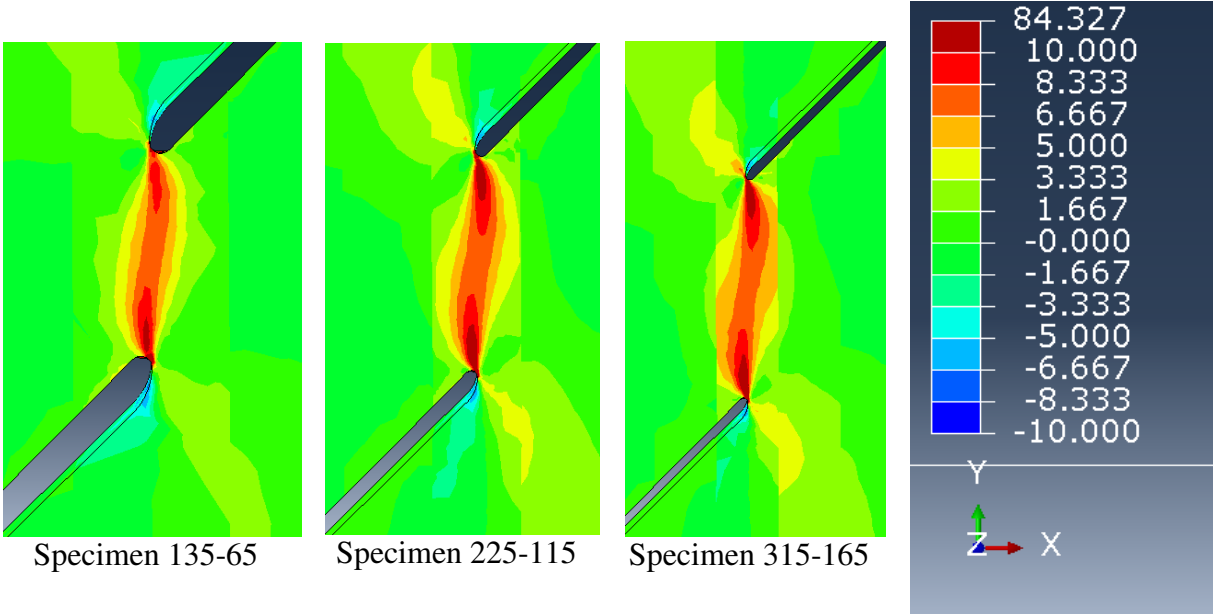


**Figure 18: Contour plots of surface shear  $\tau_{XY}$  for glulam of 45 mm lamina used for laboratory testing in part one**

Normal stress perpendicular to fibres for the three same specimens is shown in figure 19. Tension and compression normal fibre occurs around the ends of the cuts; the red areas show tension while the blue areas show compression.

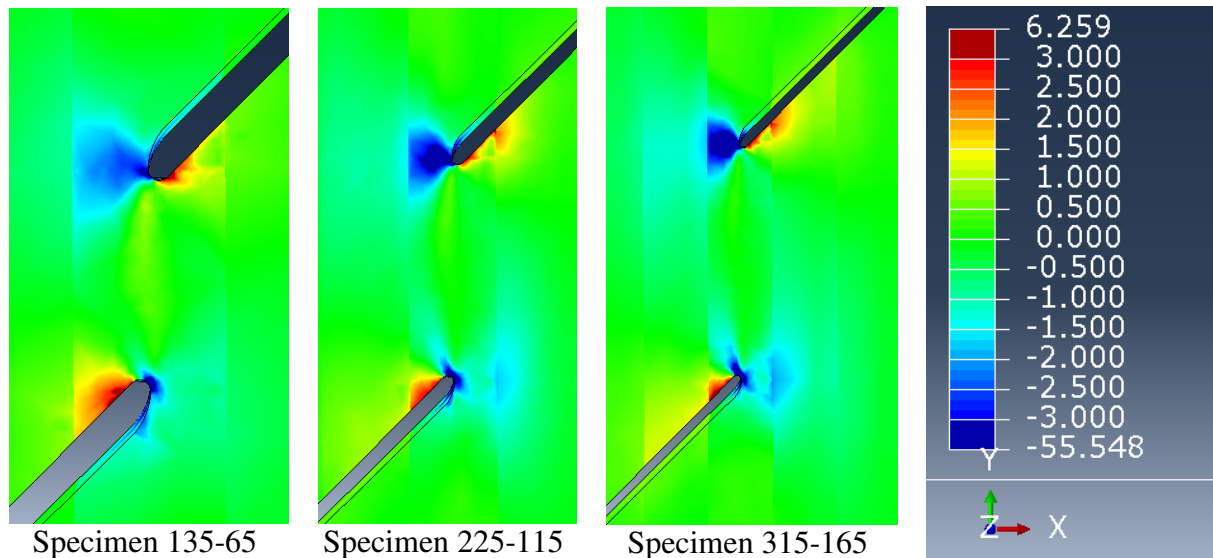


**Figure 19: Contour plots of surface normal stress  $\sigma_x$  for glulam of 45 mm lamina used for laboratory testing in part one**

### Laboratory testing

A total of nine specimens were made for testing in part one; three identical copies of specimens 135-65, 225-115 and 315-165.

The specimens were loaded continuously at a constant velocity until failure. The velocity of load application was set to 0.6 mm/min. This is a compromise between various sources. ASTM D143 (1984) says the notched shear block test should be loaded continuously at 0.6 mm/min. The European Standard EN 408 (2003) states that the failure should happen within  $300 \pm 120$  s for a shear test, while SKOGFORSK (1992) says within  $105 \pm 15$  s.

The testing was monitored by video extensometry as described earlier in this report.

### Results of testing

The moisture content of the specimens from part one varied between 9.7 % and 11.4 %, with an average of 10.81 %. The density varied from  $417 \text{ kg/m}^3$  and  $544 \text{ kg/m}^3$  with an average of  $475 \text{ kg/m}^3$ .

For all specimens, two vertical cracks formed between the cuts instead of one shear plane. This is shown in figure 20. None of the specimens split in half.



**Figure 20: Two vertical cracks forming between cuts**

The distance between the cracks was measured for all specimens. This distance increased as the height of the shear plane increased. An average value was found for the three different heights of the shear planes as shown in table 3.

**Table 3: Average values of distance between cracks for specimens in part one**

SPECIMEN NO.	TOTAL DISTANCE BETWEEN CRACKS (mm)
135-65	11,38
225-115	19,92
315-165	21,64

The maximum applied load,  $F_{max}$ , is obtained for each specimen during testing and divided by the estimated area of the shear plane,  $A_{shear,est} = h * D$ , to obtain an estimated value of the shear strength. The characteristic value (5-percentile) of the strength is calculated according to NS-EN 14358 (2006). The values are shown in table 4.

**Table 4: Mean shear strength, standard deviation, coefficient of variation and characteristic shear strength for specimens in part one**

SPECIMEN NO.	MEAN STRENGTH (Mpa) $f_{v,mean}$	STANDARD DEVIATION $s$	COEFFICIENT OF VARIATION COV	CHARACTERISTIC SHEAR STRENGTH (Mpa) $f_{v,k}$
135-65	5,84	0,54	0,0924	4,38
225-115	5,76	1,47	0,2558	2,64
315-165	5,42	0,32	0,0582	4,62

The surface examined by video extensometry must be properly lighted in order for the computer program ARAMIS to be able to generate results from the pictures. Unfortunately, for part one, the lighting on the specimens while testing was too bad, and ARAMIS could not calculate strains on the surface of the specimen. Hence, the elastic shear modulus, which is a function of strains, was not calculated in part one.

## Discussion

The two cracks that formed had their origin from the base of the upper and lower cut. Moving the cuts deeper into the specimen and making them overlap in the vertical direction while maintaining the height of the shear plane is expected to close the gap between the two cracks and form only one shear plane. This is illustrated in figure 21.

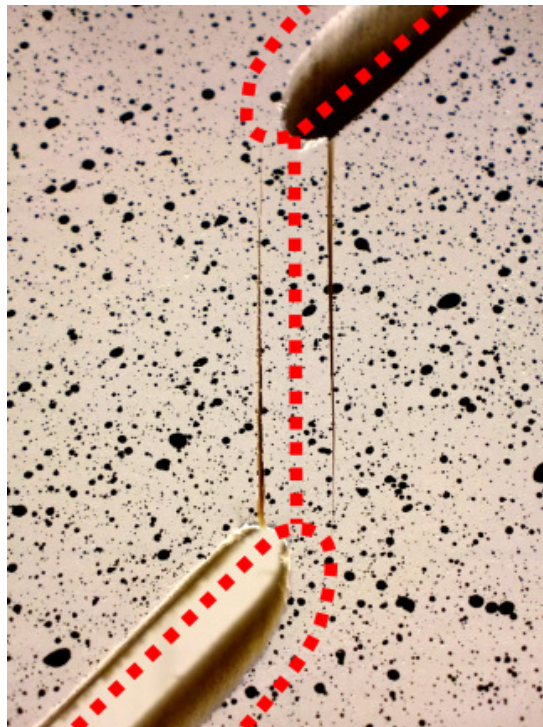


**Figure 21: The red dashed line illustrates how the cuts should be moved deeper into the specimen in order to form one shear plane instead of two cracks**

From results shown in table 3, it seems appropriate to move the cuts a total distance of between 11 - 22 mm deeper into the specimen.

From the mean values of shear strength in table 4, a size-effect is observed; the mean strength decrease by increasing shear area. A larger coefficient of variation is found for specimen 225-115 than for the other two, which increase its characteristic value. The reason for this variation is that one of the three copies of specimen 225-115 had a significant larger shear capacity than the other two; 7.4 MPa (compared to 4.4 and 4.6 MPa for the other two).



## Part two

### Numerical modelling

The three specimens from part one were modelled exactly the same way in this part, only moving the cuts deeper into the specimen in horizontal direction; a total of 20 mm (10 mm from each side) as shown in figure 22. Considering the results of the first laboratory testing, this would be sufficient overlap for all specimens to form one shear plane instead of two cracks.

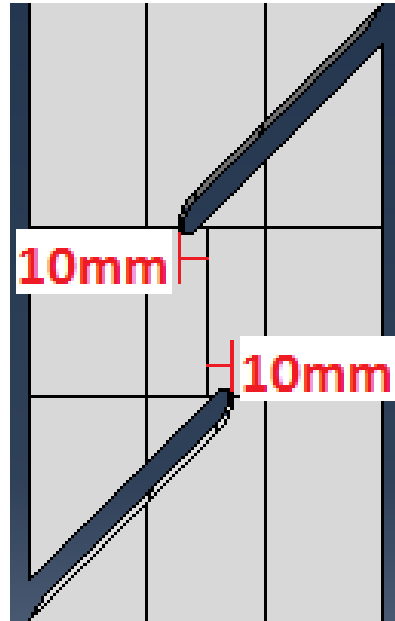
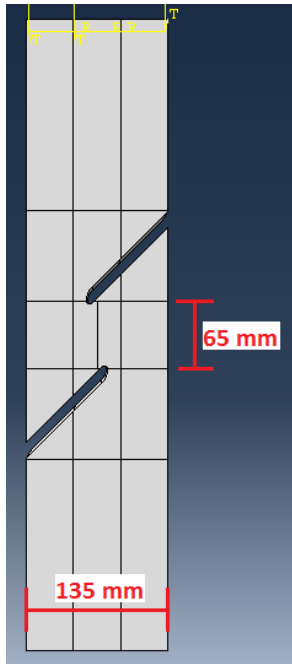
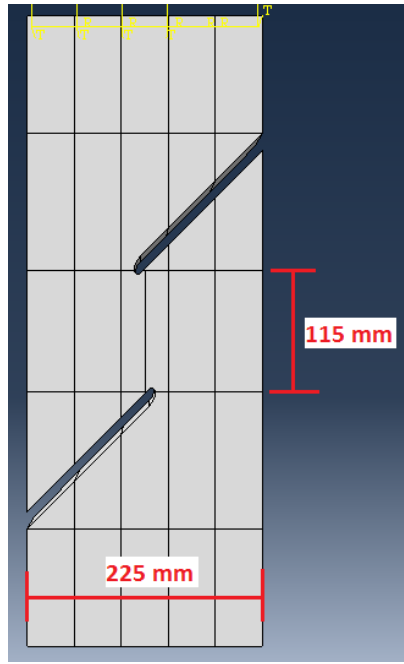


**Figure 22: Cuts moved to overlap each other by 20 mm in horizontal direction**

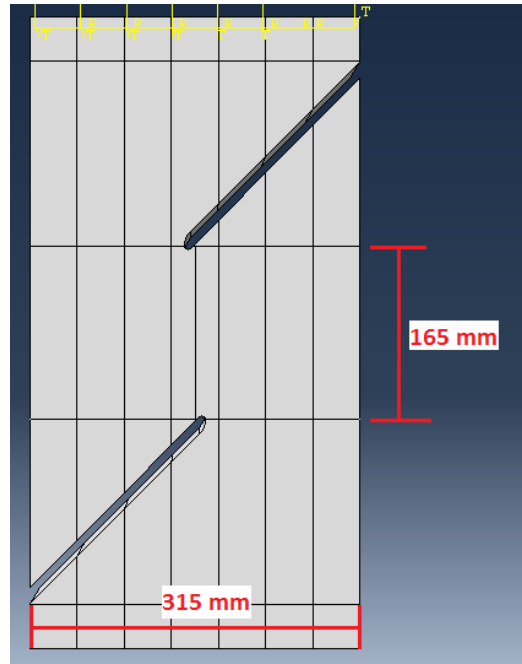
Additionally, a new, larger specimen was modelled and tested. This specimen was 800 mm high, 405 mm thick, 90 mm deep and the height of the shear plane was 200 mm. As for the other specimens, the cuts were moved 10 mm deeper into the specimen on each side. The four specimen modelled in part two are shown in figure 23. The specimen were named after their dimensions as before, adding "10x2" to indicate that the cuts were moved. All specimens were loaded until  $\tau_{xy} \sim 10 \text{ MPa}$  on the shear plane.



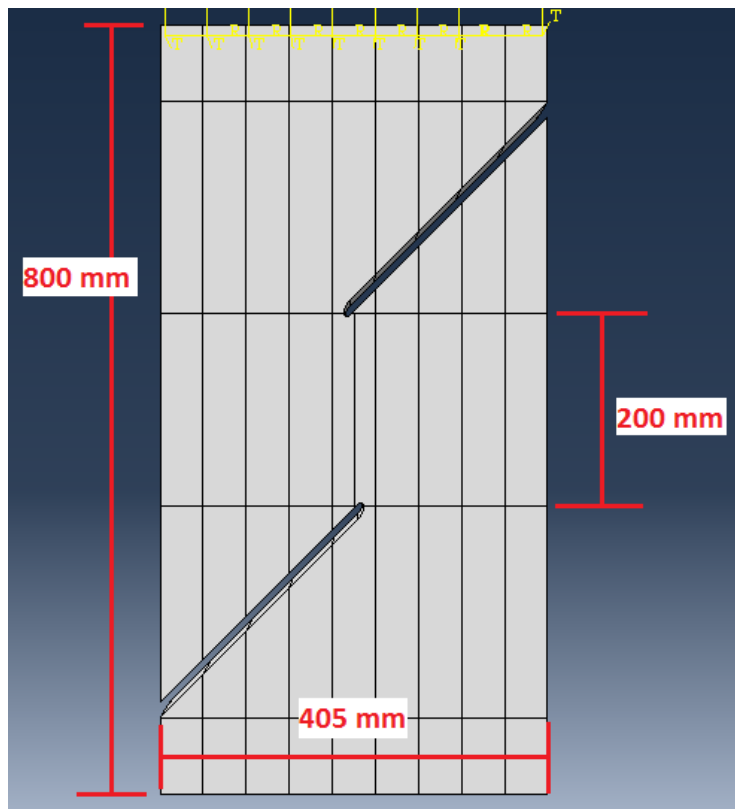
Specimen 135-65-10x2



Specimen 225-115-10x2



Specimen 315-165-10x2



Specimen 405-200-H800-10x2

Figure 23: Specimen modelled in part two

### Results of modelling

Contour plots of the shear stress are plotted below in figure 24. The shear distribution along the height of the shear plane is well distributed, but has an inclination in vertical direction for the smallest specimens.

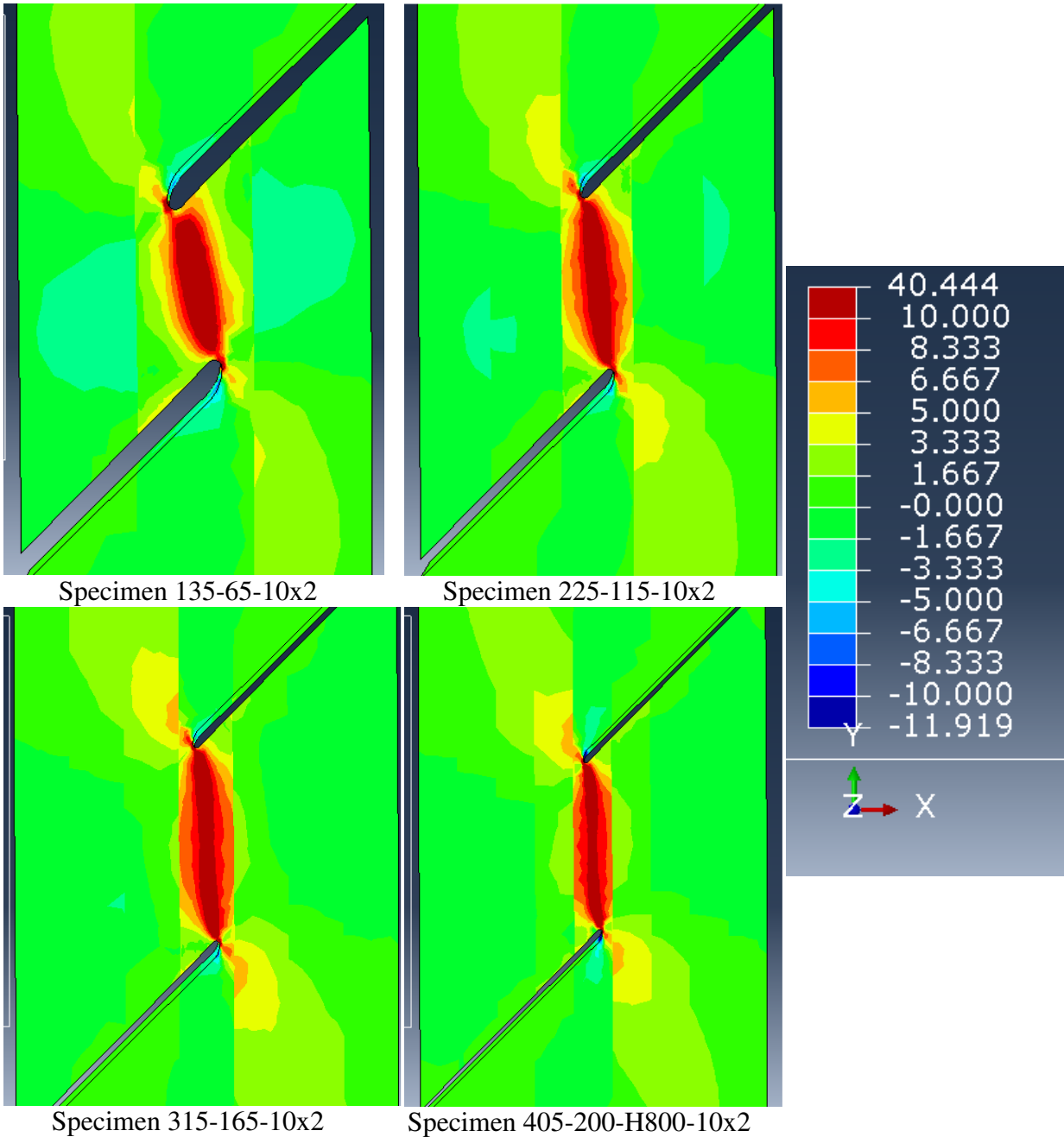
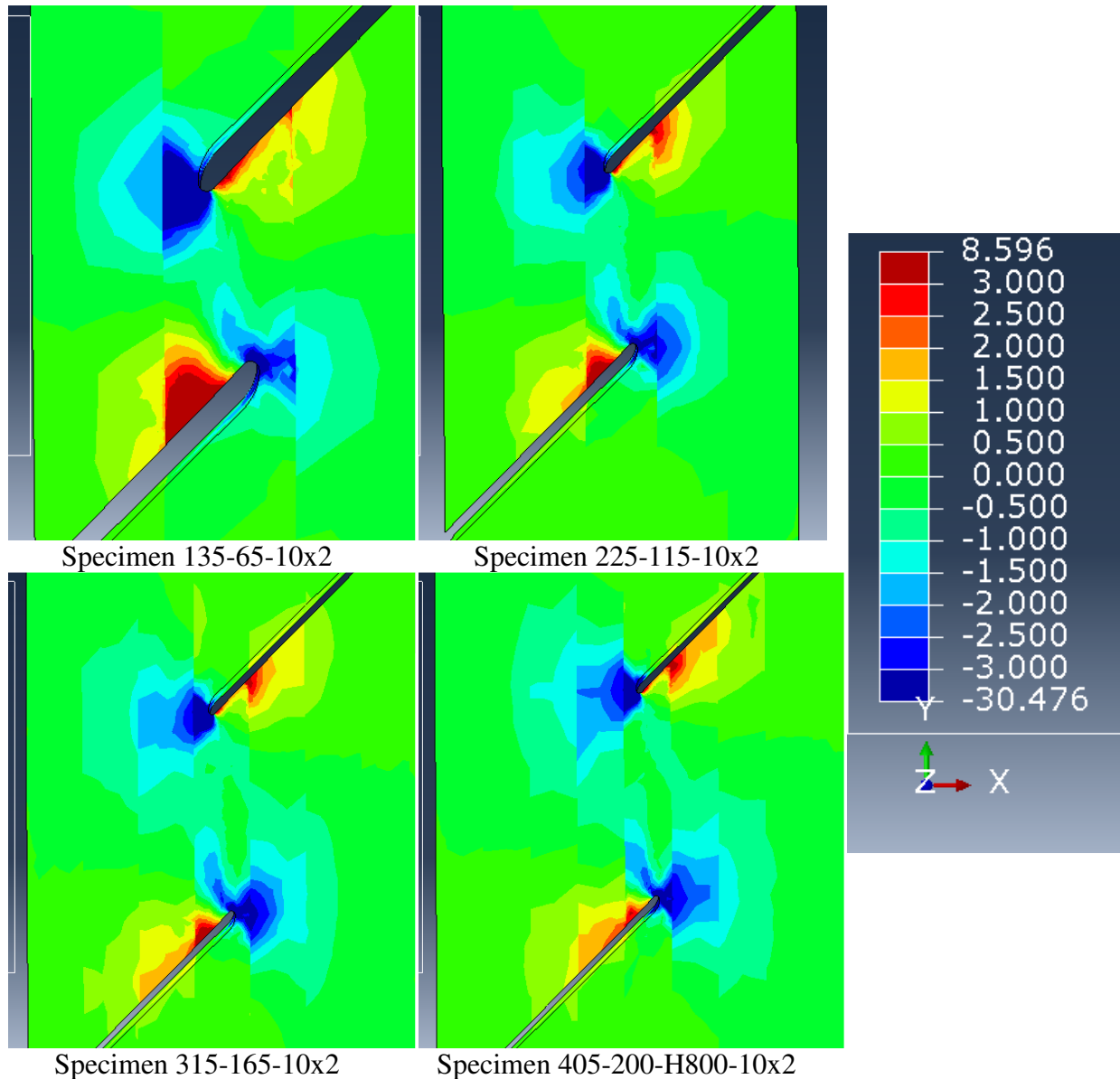


Figure 24: Contour plots of surface shear stress for specimens in part two

The normal stress distribution perpendicular to fibres is shown in the contour plots in figure 25. As for part one, there are areas of tension (red) and areas of compression (blue) along the cuts.



**Figure 25: Contour plots of normal stress perpendicular to fibres for specimens in part two**

### Laboratory testing

Three identical copies of each of the four specimens modelled above were tested in the laboratory, which makes a total of twelve specimens tested in part two. The procedure of testing was not changed from part one; the specimens were continuously loaded at 0.6 mm/min until failure. Video extensometry was used during testing.

### Results of testing

The moisture content of the specimens from part two varied between 10.6 % and 13.14 %, with an average of 11.83 %. The density varied from 366 kg/m<sup>3</sup> and 576 kg/m<sup>3</sup> with an average of 482 kg/m<sup>3</sup>.

Approximately 60 % of the specimens split in half at failure, exposing one shear plane as shown in figure 26. The remaining 40 % of the specimens formed two cracks with origin from the cuts; see figure 27. 60 % of the specimens which split in half also had cracks along the sides of the shear plane as shown in figure 28.



**Figure 26: Specimen split in half at failure forming one shear plane**



**Figure 27: Two cracks formed at failure**

**Figure 28: Specimen split in half by shear but also forming cracks along the sides.**

Typical contour plots from ARAMIS of shear strains and normal strains perpendicular to fibres are shown in figures 29 and 30. The plots from ARAMIS are compared to plots from ABAQUS with approximately the same shear stress applied to the shear plane. The ABAQUS plots are shown in figures 31 and 32. The numerical results and the results from laboratory testing have a striking resemblance.

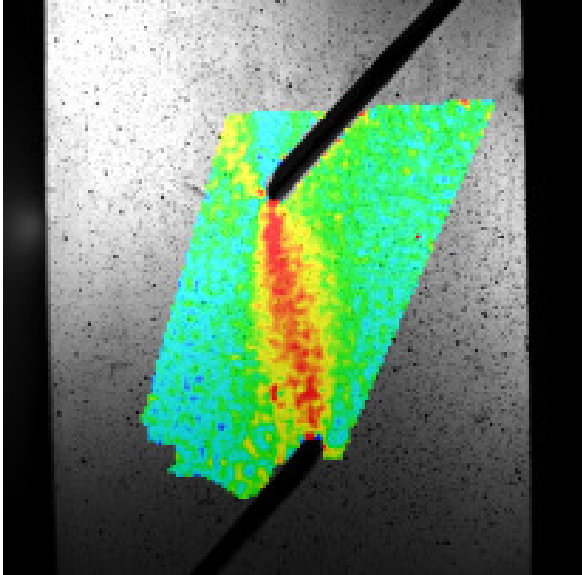


**Figure 29: Typical contour plot of shear strains from ARAMIS**

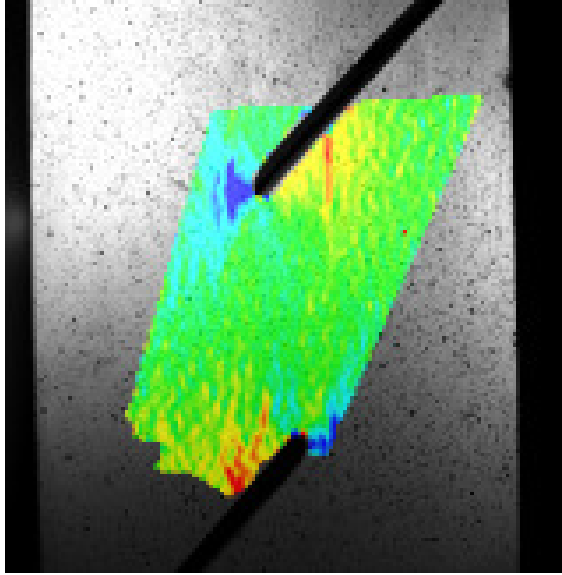


**Figure 30: Typical contour plot of normal strains perpendicular to fibres from ARAMIS**

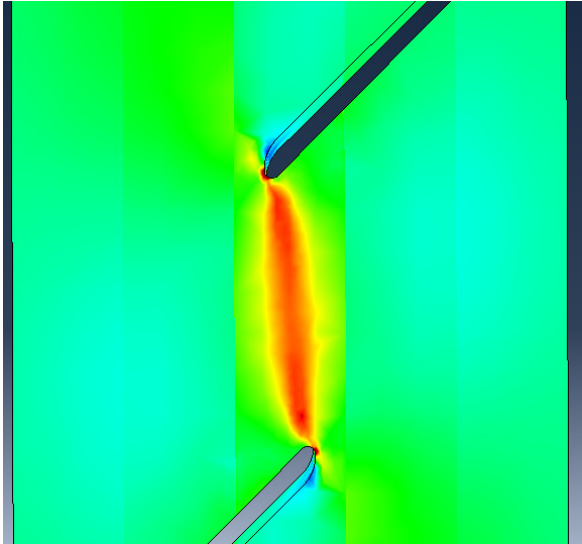


**Figure 31: Typical contour plot of shear strains from ABAQUS**

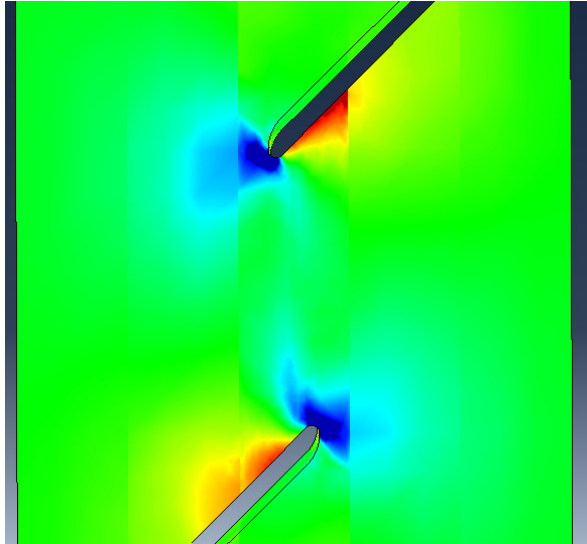


**Figure 32: Typical contour plot of normal strains perpendicular to fibres from ABAQUS**

A path along the height of the shear plane was added to the ABAQUS and ARAMIS contour plots of shear strain and normal stress perpendicular to fibres, as shown in figures 33 and 34, in order to plot the distribution of strain against the height of the shear plane. The path for

shear strains are centred in the middle of the specimens, while the path for normal strains origin from the area around the upper cut with largest concentration of tension.

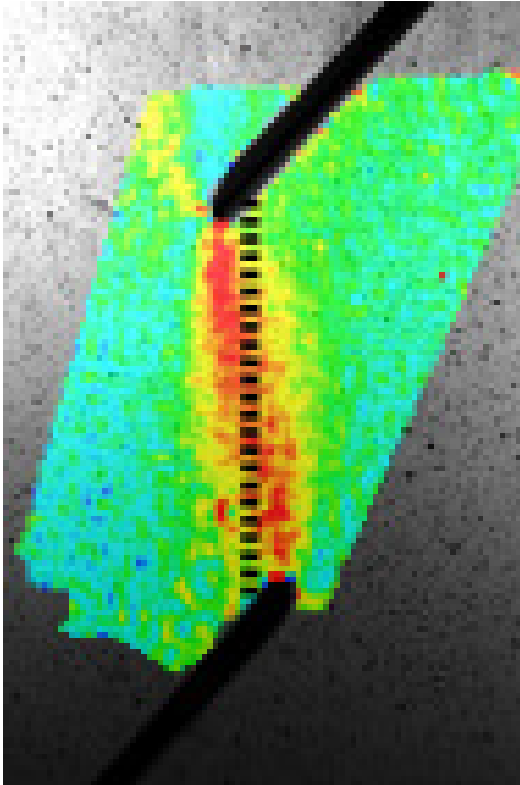


**Figure 33: Path used for plotting of shear strains**

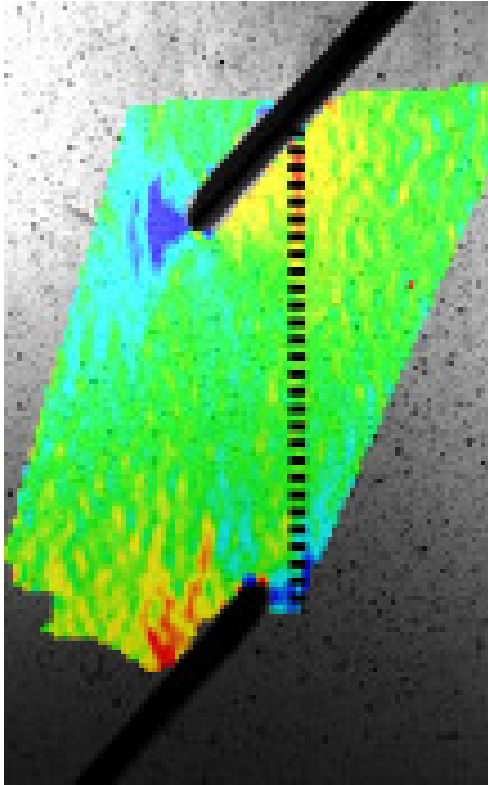


**Figure 34: Path used for plotting of normal strains perpendicular to fibres**

The distributions are shown in figure 35 for shear strain and figure 36 for normal strain from ABAQUS and ARAMIS contour plots for an incidental specimen.

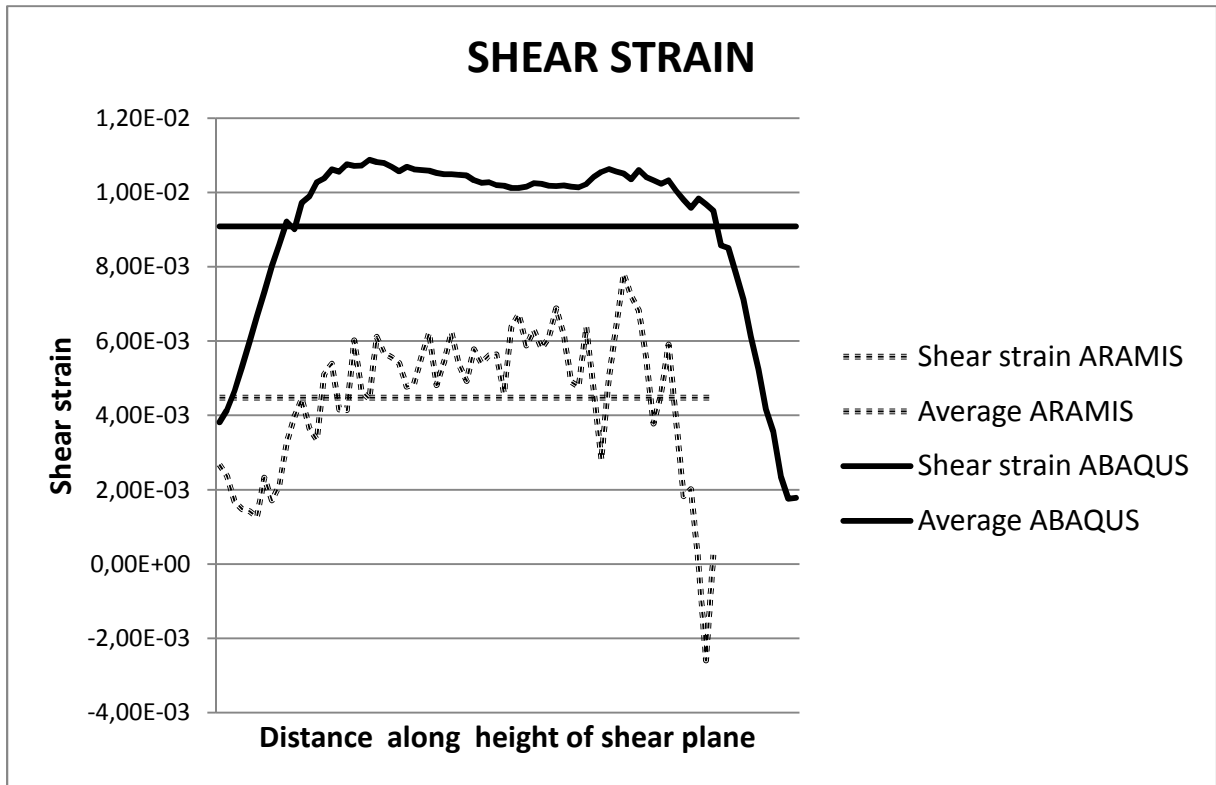


Figure 35: Shear strain from ARAMIS (dotted) and ABAQUS (solid) plotted against the height of the shear plane

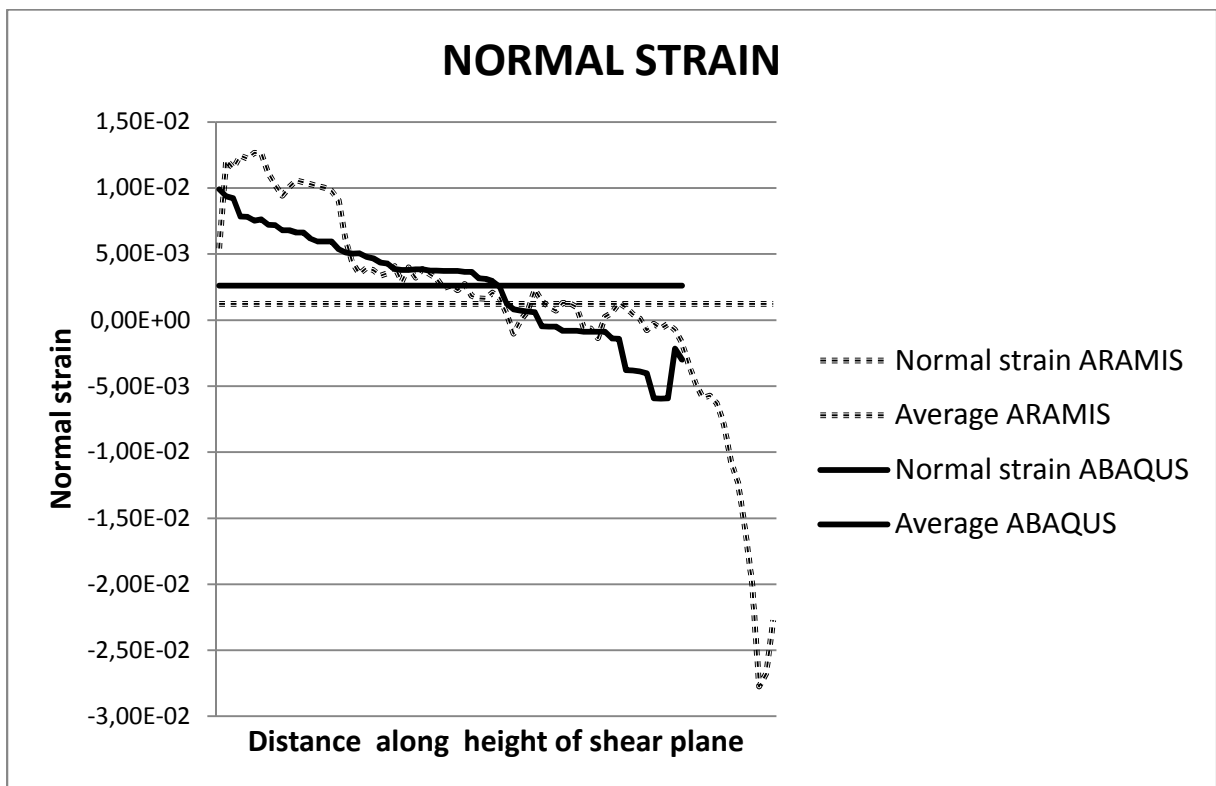
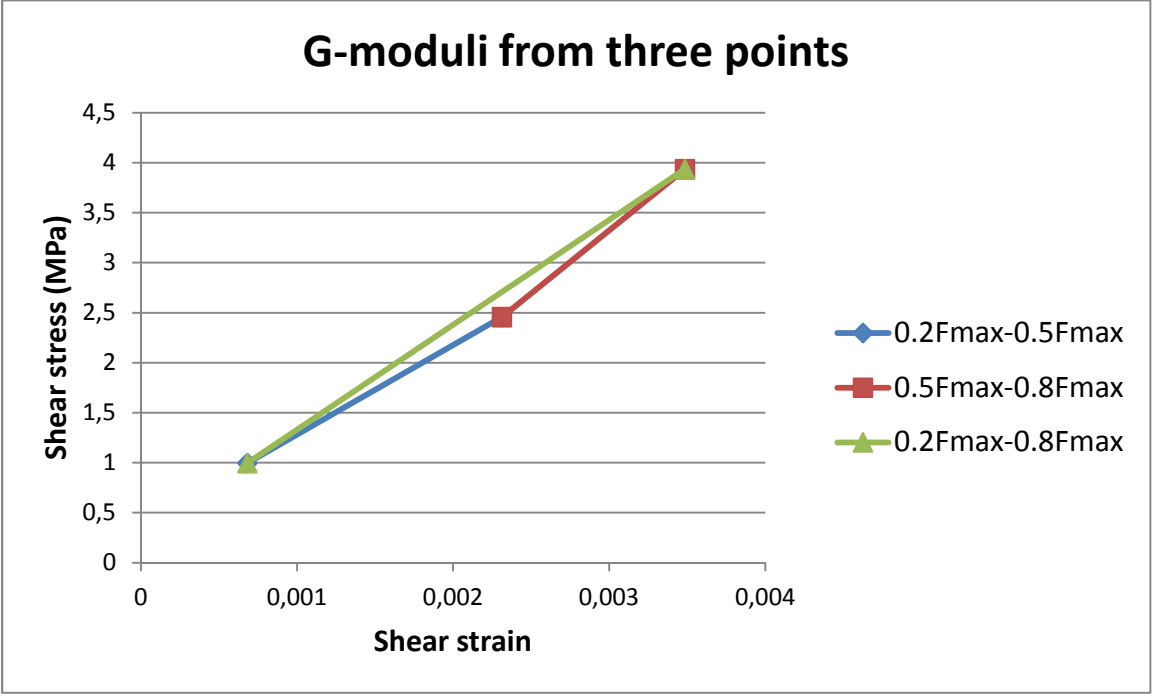


Figure 36: Normal strain perpendicular to fibres from ARAMIS (dotted) and ABAQUS (solid) plotted against the height of the shear plane

The average shear strain was calculated from ARAMIS-data for three points from the loading history;  $0.2F_{max}$ ,  $0.5F_{max}$  and  $0.8F_{max}$ . These three values for average strain were plotted against the corresponding load ( $0.2F_{max}$ ,  $0.5F_{max}$  and  $0.8F_{max}$ ) as shown in figure 37. Linear interpolation is performed between two and two points to obtain three values of the G-modulus.



**Figure 37: Average strain at  $0.2F_{max}$ ,  $0.5F_{max}$  and  $0.8F_{max}$  with G-modulus as the difference quotient between each point**

Averages of the three temporary G-moduli in figure 37 are calculated as an estimate of the elastic G-modulus for specimens in part two. The results for all specimens are shown in table 5.

**Table 5: Mean values of G-modulus for specimens in part two**

<u>SPECIMEN NO.</u>	<u>G<sub>mean</sub></u>
<u>135-65-10x2</u>	<u>873,66</u>
<u>225-115-10x2</u>	<u>1 072,05</u>
<u>315-165-10x2</u>	<u>916,45</u>
<u>405-200-H800-10x2</u>	<u>1 069,64</u>

The mean values of the shear strength were also calculated by dividing the maximum applied load by the shear area. The results are shown in table 6 and shows a tendency to have a size-effect, but not as clear as for results from part one.

**Table 6: Mean shear strength for specimens in part two**

SPECIMEN NO.	MEAN STRENGTH (Mpa)
	$f_{v,mean}$
135-65-10x2	4,04
225-115-10x2	5,00
315-165-10x2	3,67
405-200-H800-20x2	4,85

*The coefficient of variation and the characteristic values of shear strength and stiffness for a merger of part two and three are calculated later in this report.*

The specimens with the two largest dimensions formed vertical cracks from top and base before the shear zone fractured, as shown in figure 38.



**Figure 38: Cracks forming from top of specimen**

The results from one of the largest specimens were excluded because it fractured due to cracks forming from top.

### **Discussion**

As shown above, the specimens formed either one shear plane and split in half or formed two cracks along the sides of the shear plane. Compared to the contour plots from both ABAQUS and ARAMIS, it is seen that the cracks origin from the area along the cuts with

concentrated tension perpendicular to fibres. This might mean that 40 % of the specimens failed due to tension perpendicular to fibres. The remaining 60 % of the specimens formed a shear plane and split in half at failure, but 60 % of these also formed two cracks. It is difficult to establish whether the fracture of these specimens is due to shear stress or tension perpendicular to fibres or a combination of these two. If some of the specimens failed due to tension perpendicular to fibres, this will have an influence on the shear capacity calculated in table 6; some of the values might be too low because the specimen failed due to tension before the shear capacity was reached, which means that the shear capacity might be underestimated.

The stiffness computed for specimens in part two is high compared to values from literature (see figure 5). It is suspected that this might have the simple explanation that the method used for estimation of shear stiffness was too simplified. In their report, Dahl and Malo (2009a) plotted the shear strain against stress forming a continuous line for the whole test-period as shown in figure 39. The shear modulus was found as the difference quotient of this line, using a least sum square error (SSE) optimization to fit the linear elastic shear moduli estimate to the observed stress-strain relationships. The shear modulus is seen in figure 39 as a thin, white line on the black line. This method gave good values for the G-modulus compared to literature.

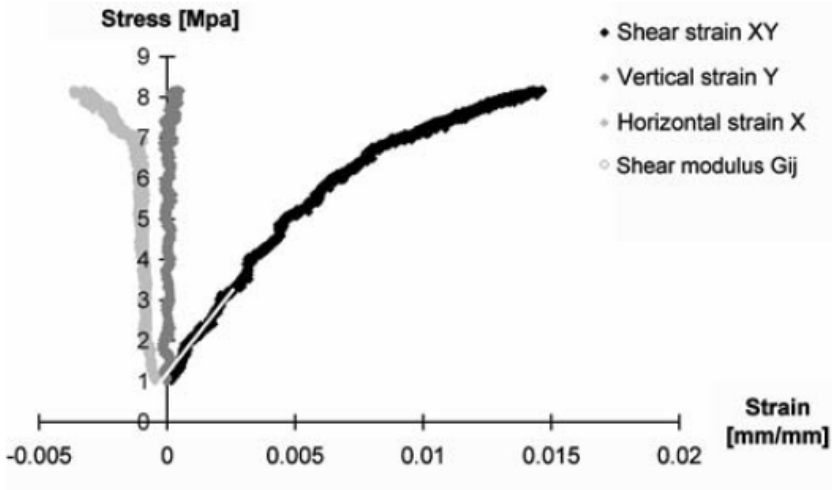


**Figure 39: Shear strain (black line) is plotted against stress (Dahl and Malo, 2009a)**

Only three values along the stress-strain path were calculated in this report due to lack of time. A proper method, like the one used by Dahl and Malo (2009a), might be needed in order to obtain better values for the G-moduli.

Concerning the two largest specimens, which formed cracks from top and base, no significant difference in contour plots from ABAQUS showing shear stress, normal stress parallel to fibres and perpendicular to fibres is observed between the smallest specimens

and the largest specimens. Looking at specimen dimensions, the most significant difference from the smallest to the largest specimen is the length of solid wood above (or below) the cuts, along the edge of the specimen. It is suspected that the total height of the largest specimens might be too small; the compression load might have too little space to distribute from the top to the shear plane without producing too large bending moments. Hence, it is desirable to increase the total height of the largest specimens. Figure 4 shows the dimensions of a general specimen.

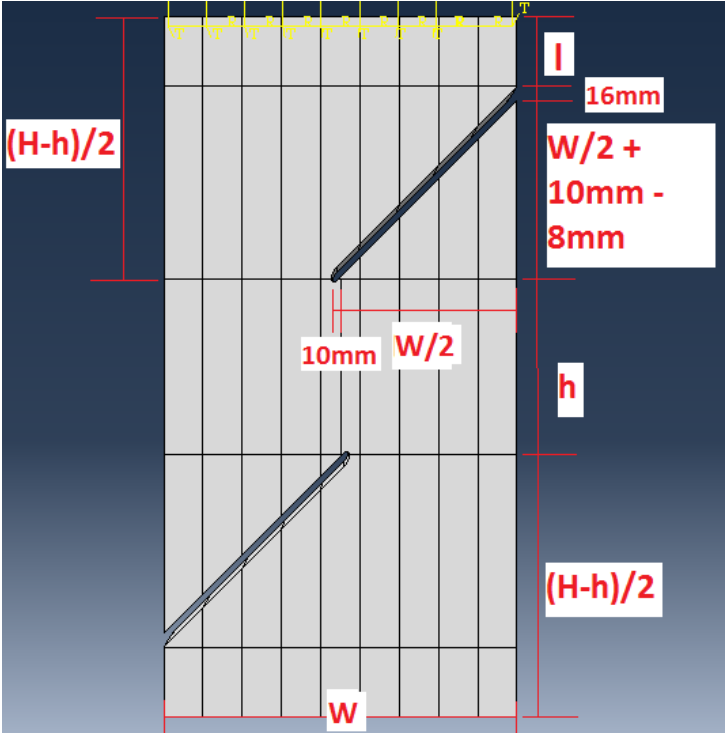


Figure 40:

- **W = Width = 9 x 45 mm = 405 mm for all specimens**
- **D = Depth = 90 mm for all specimens**
- **H = Height of specimen**
- **h = Height of shear plane**
- **l = length of solid wood above cut (or below cut for left cut)**

Only the two specimens with largest dimensions form cracks from top or base of specimen. Hence, the length, l, along the edge of the specimen above the cuts is decided to have a lower limit of 112 mm as used for the second smallest specimen. The total height of the specimen is calculated from the following formula:

$$\frac{H - h}{2} = \frac{W}{2} + 10 \text{ mm} + 8 \text{ mm} + l$$

$$\xrightarrow{\text{yields}} H = W + (2 * 10\text{mm}) + (2 * 8\text{mm}) + 2l + h \quad (4)$$

Calculating the length  $l$  for all specimens in part two, and also the ratio  $h/l$  gives results as shown in table 7.

**Table 7: Length  $l$  and ratio of  $h/l$  calculated for specimens in part two**

***From Lab Part 2:***

SPECIMEN NO.	$h$ (mm)	$H$ (mm)	$W$ (mm)	$l$ (mm)	Ratio $h/l$
135-65-10x2	65	600	135	182	0,357142857
225-115-10x2	115	600	225	112	1,026785714
315-165-10x2	165	600	315	42	3,928571429
405-165-H800-10x2	200	800	405	79,5	2,51572327

It is seen from table 7 that a ratio  $h/l < 1,026785714$  must be used in order for  $l$  to be large enough if the assumption that the second smallest specimen has sufficient height is correct.



## Part three

### Numerical modelling

The position of the cuts and the height of the shear plane were exactly like in part two; cuts overlap by 20 mm and  $h = 65$  mm, 115 mm, 165 mm and 200 mm. However, two changes were made regarding the width,  $W$ , and the total height,  $H$ , of the specimens: For part three, all specimens were 405 mm wide. The total heights of the specimens increase with increasing height of shear plane as discussed in part two. The total height is calculated below.

For constant width  $W = 405$  mm and by choosing  $h/l = 1$ , which yields  $l = h$ , the total height of the specimens can be calculated from equation 4 derived in part two:

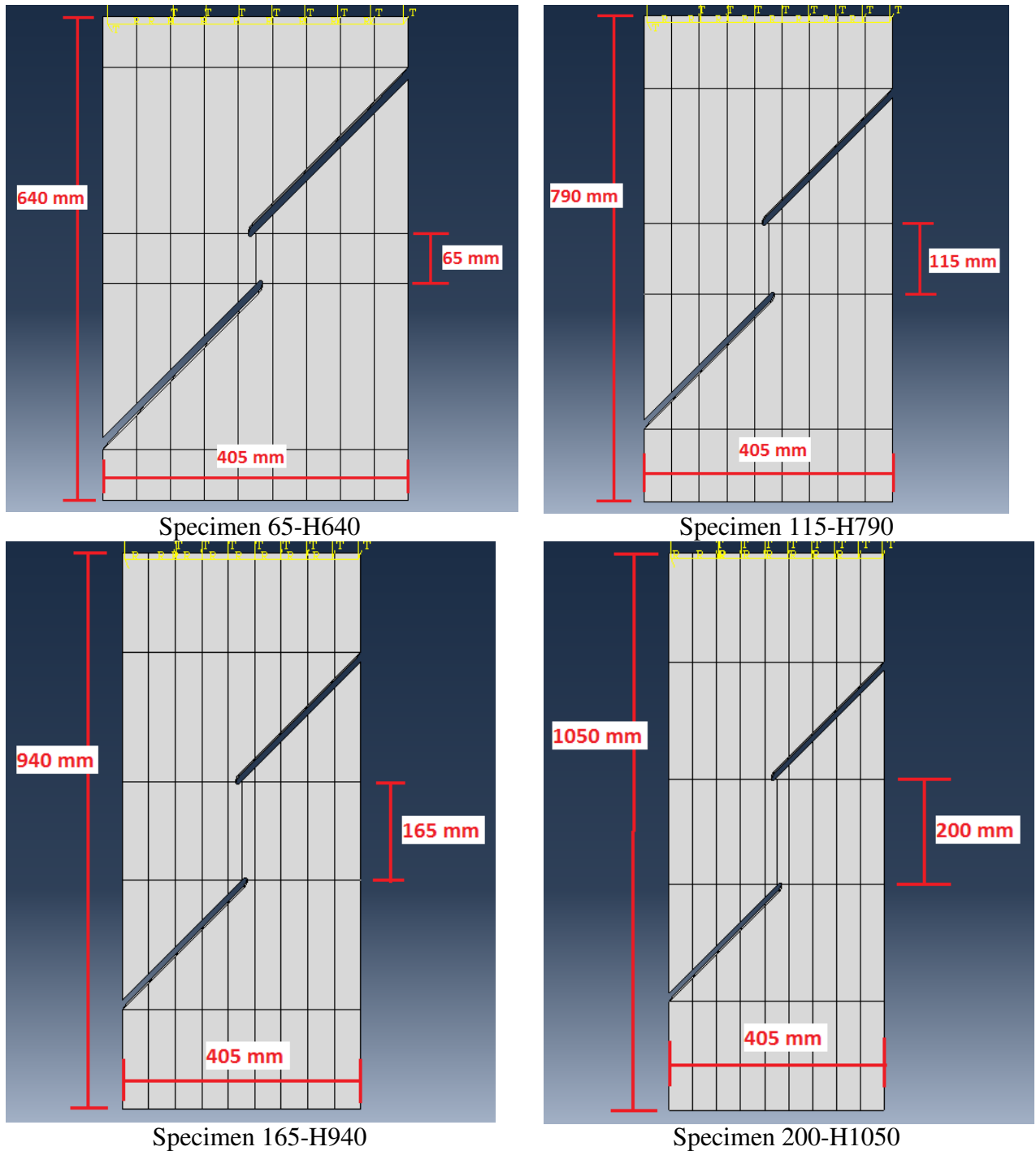
$$H = W + (2 * 10mm) + (2 * 8mm) + 2l + h = 441 \text{ mm} + 3h$$

Table 8 shows the minimum value of the total height,  $H$ , for different specimens in part three.

**Table 8: Total height,  $H$ , used for specimens in part three**

SPECIMEN NO.	$h$ (mm)	$H$ must be larger than:	<b><math>H</math> (mm) used for new specimens</b>
65-H640	65	636	<b>640</b>
115-H790	115	786	<b>790</b>
165-H940	165	936	<b>940</b>
200-H1050	200	1041	<b>1050</b>

The four specimens modelled in part three are shown in figure 41.



**Figure 41: Specimens modelled in part three**

As before, the analysis ran until  $\tau_{xy} \sim 10 \text{ MPa}$  on the shear plane.

### Results of modelling

The contour plots of surface shear stress for specimens in part three are shown in figure 42. No significant difference is observed compared to plots from part two; the smallest specimens have an inclination on the distribution of shear along the height of the shear plane.

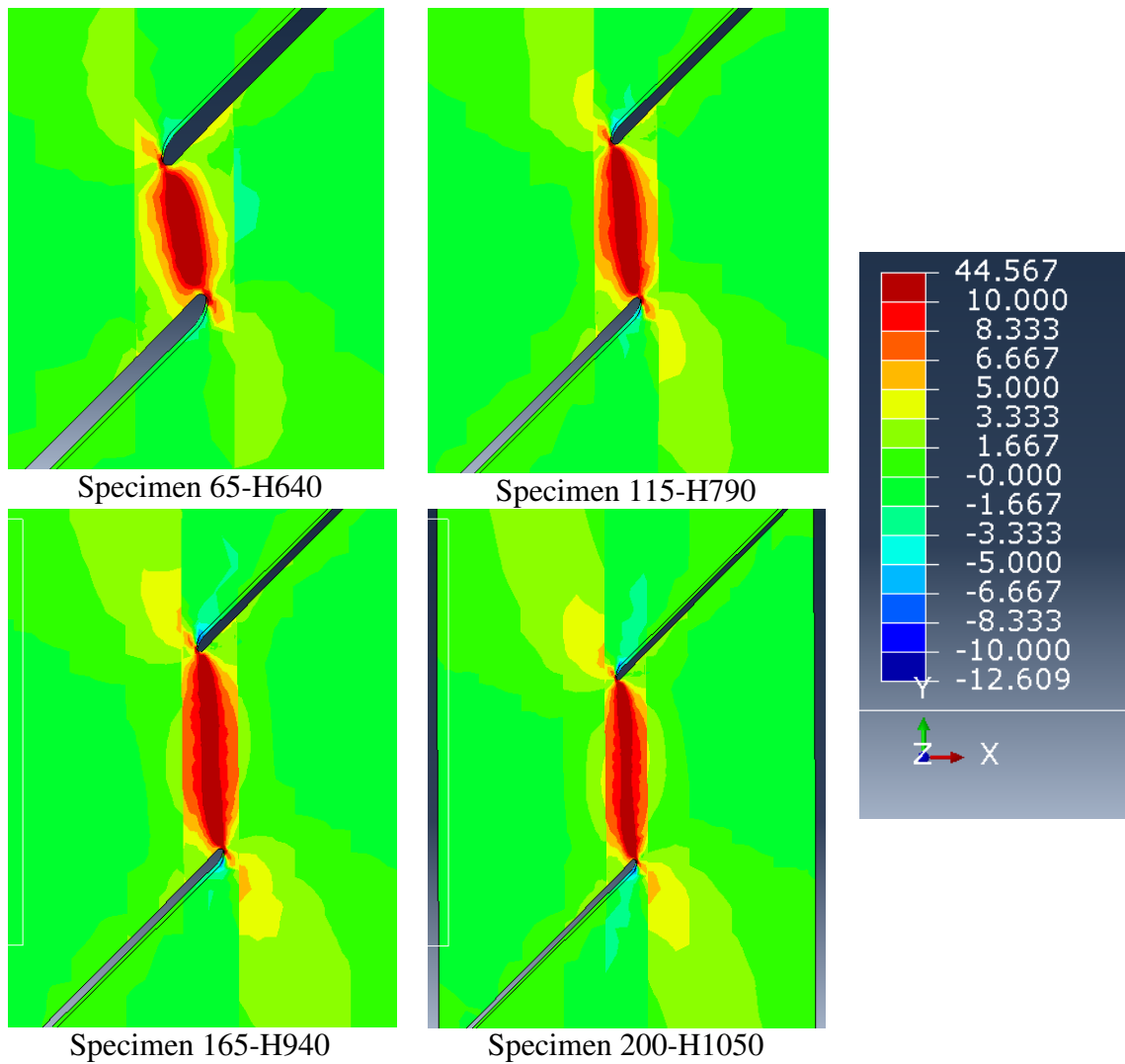


**Figure 42: Contour plots of surface shear stress for specimens modelled in part three**

Contour plots of normal stress perpendicular to fibres are plotted in figure 43. There are areas with concentration of tension (red) or compression (blue) as in part two.

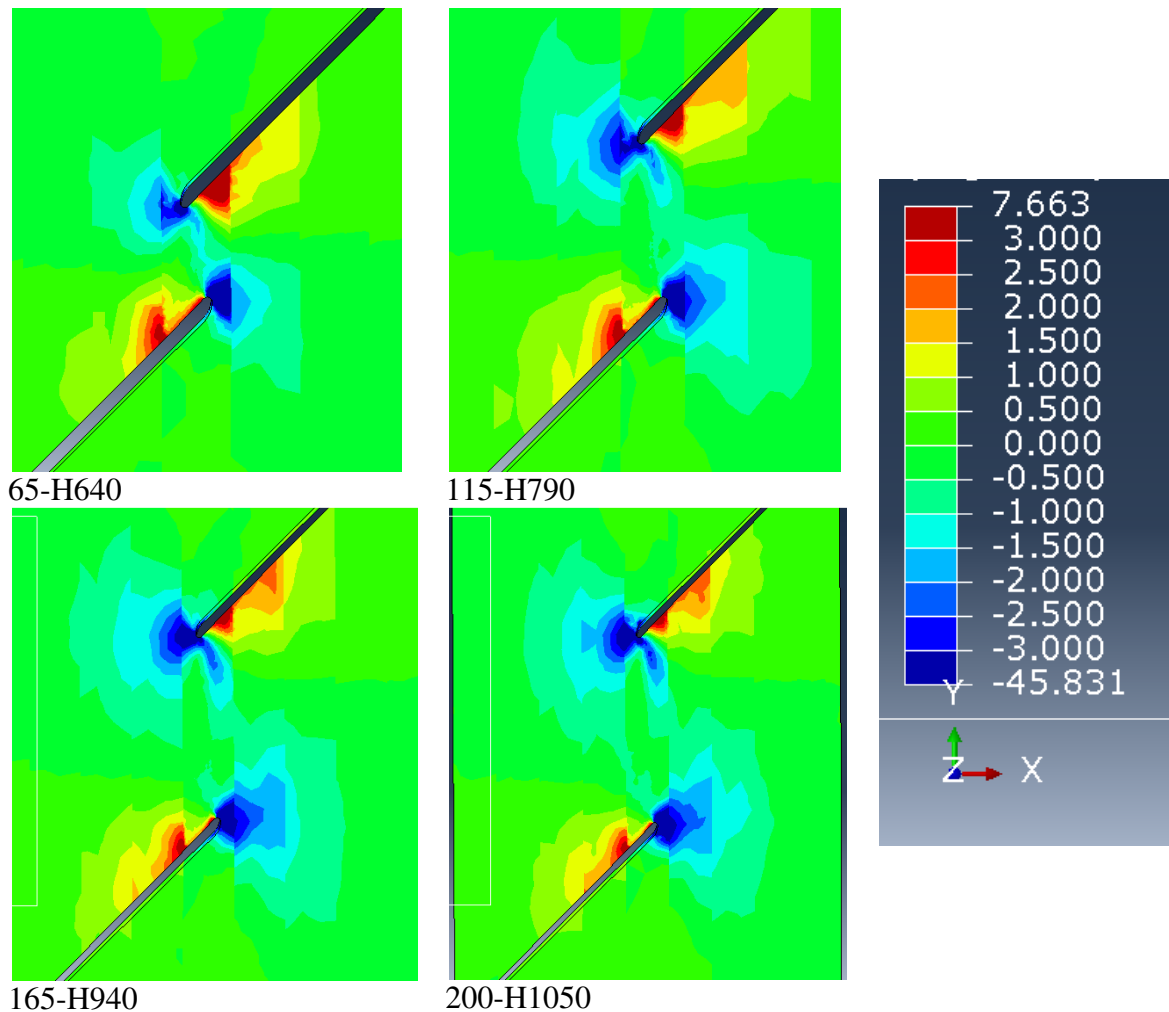


**Figure 43: Contour plots of surface normal stress perpendicular to fibres for specimens modelled in part three**

### Laboratory testing

Nine copies of the smallest specimen (65-H640), eight copies of the two middle sized specimens (115-H790 and 165-H940) and eleven copies of the largest specimen (200-H1050) were made and tested. Hence, a total number of 36 specimens were tested in part three.

The specimens were loaded continuously until failure as before, the loading being applied at a constant velocity of 0.6 mm/min. Video extensometry were used to measure surface strains.

### Results of testing

The moisture content of the specimens from part three varied between 9.9 % and 13.0 %, with an average of 11.3 %. The density varied from 379 kg/m<sup>3</sup> and 591 kg/m<sup>3</sup> with an average of 480 kg/m<sup>3</sup>.

One specimen of dimensions 165-H940 was broken before testing, hence there was no results from this specimen. One of the largest specimens exceeded the maximum loading capacity for the test machine (100 kN) and did not fracture. For two of the smallest specimens, no data from the video extensometry was available. Also, one of the largest

specimens was excluded when calculating G-modulus due to very high values of surface strain from ARAMIS.

Approximately 50 % of the specimens split in half at failure, exposing one shear plane. The remaining 50 % of the specimens formed two cracks parallel to the shear plane. Practically all of the specimens which split in half also had cracks along the sides of the shear plane. These observations are very similar to the observations from part two.

The estimated mean shear strength,  $f$ , and mean elastic shear modulus,  $G$ , is calculated as described in part two. The results are shown in table 9. The size-effect on shear strength is noticeable also in part three.

**Table 9: Mean shear modulus and G-modulus estimated for part three**

<b>SPECIMEN NO.</b>	<b><math>f_{mean}</math></b>	<b><math>G_{mean}</math></b>
<b>65-H640</b>	4,85	1 174,36
<b>115-H790</b>	4,75	1 057,57
<b>165-H940</b>	3,99	1 125,19
<b>200-H1050</b>	4,03	1 242,40

*The coefficient of variation and the characteristic values of shear strength and stiffness for a merger of part two and three are calculated later in this report.*

## **Discussion**

The suspicion from part two; that the specimens fail either from shear, tension perpendicular to fibres or a combination of these two, is maintained for part three results. It is seen from the contour plots of normal stress perpendicular to fibres that the cracks have their origin from the area with large tension stresses along the cuts. Hence, the shear strength might be underestimated for part three as well.

As in part two, the estimated G-moduli are high compared to values from literature. No change in estimation method from part two is carried out; hence, these high values might have the same explanation as discussed in part two.



## Results from part two and three merged

The design of the shear-zone of specimens in part two and three is equal, and the results considered very similar; hence the results from these two parts are merged. Some specimens are rejected as described in part two and three. Also, the results from the largest specimens from part two are rejected here because the influence of the cracks forming from top and base of the specimens is expected to be relevant. This means that the results from a total number of 43 specimens are included in strength calculations and a total number of 41 specimens are included in stiffness calculations. An overview of specimens included is shown in table 10.

**Table 10: Amount of specimens included from part two and part three regarding strength and stiffness results**

<i><b>FROM PART 2</b></i>		<b>NUMBER OF SPECIMENS INCLUDED</b>	
<b>SPECIMEN NO</b>		<b>STRENGTH</b>	<b>STIFFNESS</b>
135-65-10x2		3	3
225-115-10x2		3	3
315-165-10x2		3	3
405-165-H800-10x2		0	0

<i><b>FROM PART 3</b></i>		<b>NUMBER OF SPECIMENS INCLUDED</b>	
<b>SPECIMEN NO</b>		<b>STRENGTH</b>	<b>STIFFNESS</b>
65-H640		9	7
115-H790		8	8
165-H940		7	7
200-H1050		10	10

<i><b>PART 2 AND 3 MERGED</b></i>		<b>NUMBER OF SPECIMENS; n</b>	
<b>HEIGHT OF SHEAR PLANE</b>		<b>STRENGTH</b>	<b>STIFFNESS</b>
65		<b>12</b>	<b>10</b>
115		<b>11</b>	<b>11</b>
165		<b>10</b>	<b>10</b>
200		<b>10</b>	<b>10</b>
<b>TOTAL</b>		<b>43</b>	<b>41</b>

Table 11 shows mean G-modulus, standard deviation, coefficient of variation and 5-percentile calculated for the different specimen heights of shear plane from part two and part three results. The mean value of the 5-percentile G-modulus for all 41 specimens is approximately 970 MPa. The 5-percentile is calculated according to NS-EN 14358 (2006).

**Table 11: Mean G-modulus, standard deviation, coefficient of variation and 5-percentile for specimens investigated in part two and part three**

HEIGHT OF SHEAR PLANE	MEAN G-MODULUS (MPa)	STANDARD DEVIATION	COV	5-PERCENTILE (MPa)
$h$	$G_{mean}$	$s_G$	COV(G)	$G_{05}$
65	1 084,15	266,09	0,2454	952,14
15	1 061,52	96,35	0,0908	953,13
165	1 062,57	322,51	0,3035	926,89
200	1 242,40	425,80	0,3427	1 071,79

Table 12 shows the mean values of strength, standard deviation, coefficient of variation and the characteristic 5-percentile calculated for the different specimen heights of shear plane from part two and part three results. The 5-percentile is calculated according to NS-EN 14358 (2006).

**Table 12: Mean shear strength, standard deviation, coefficient of variation and 5-percentile for specimens investigated in part two and part three**

HEIGHT OF SHEAR PLANE	MEAN STRENGTH (MPa)	STANDARD DEVIATION	COV	CHARACTERISTIC STRENGTH (MPa)
$h$	$f_{mean}$	$s_f$	COV( $f$ )	$f_{05}$
65	4,44	0,9790	0,2203	3,05
15	4,88	0,6816	0,1398	3,61
165	3,83	0,7260	0,1896	2,62
200	4,03	0,6553	0,1626	2,82

The correlation between shear strength,  $f$ , G-modulus,  $G$ , and density,  $\rho_{12}$ , is investigated. In figure 44, shear strength is plotted against density and in figure 45, G-modulus is plotted against density for all specimens included from part two and part three.

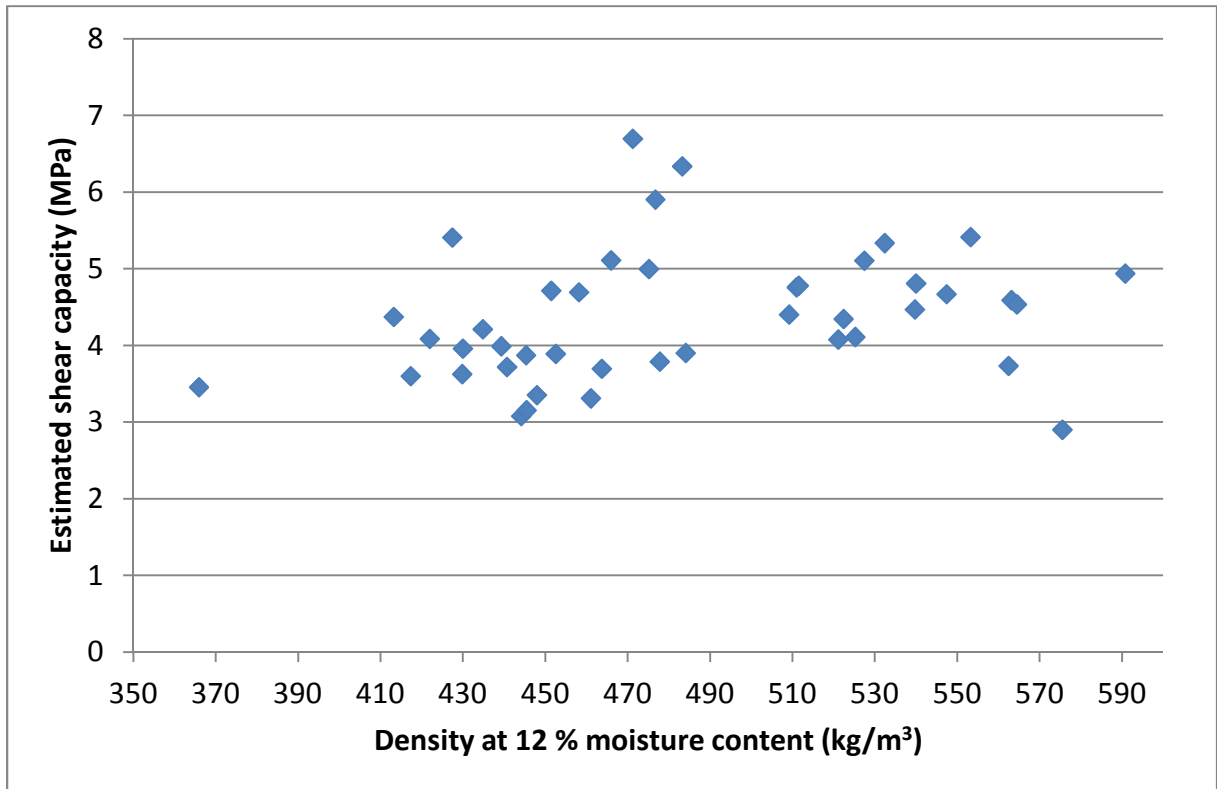


Figure 44: Estimated shear strength plotted against density

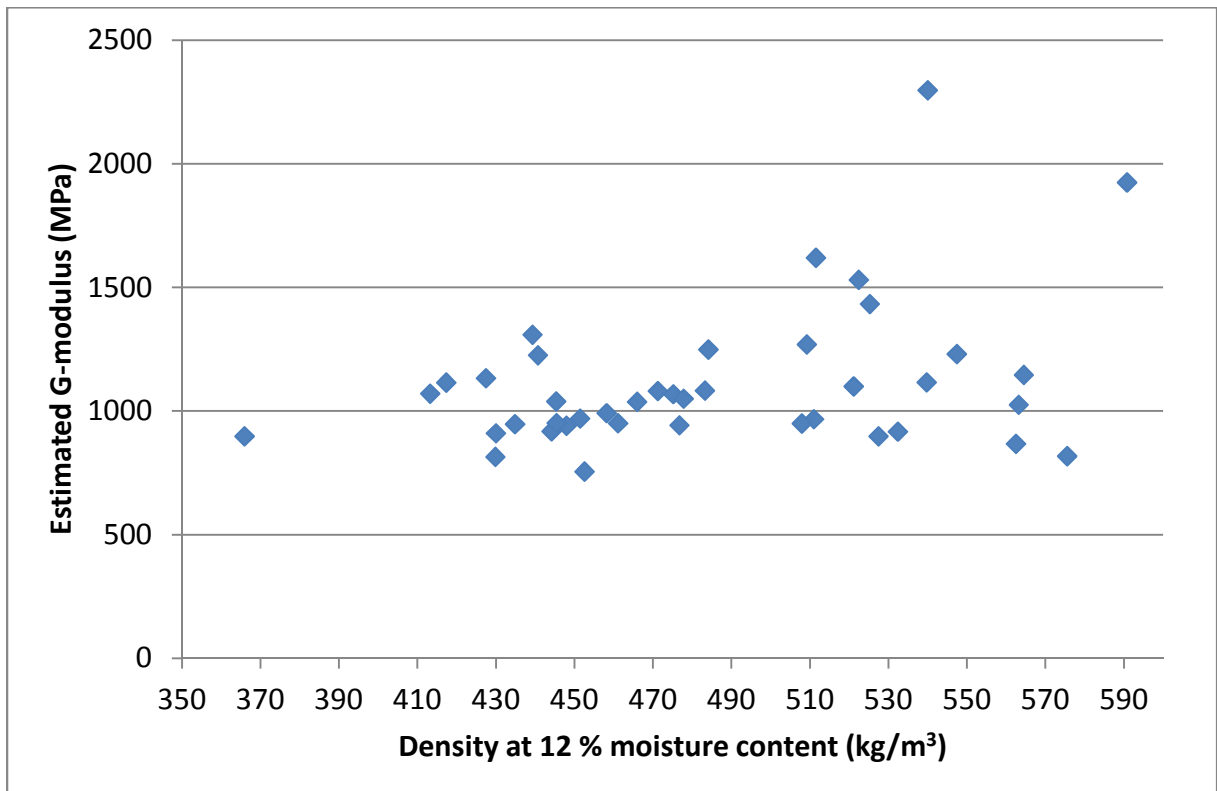


Figure 45: Estimated G-modulus plotted against density

The Pearson product-moment correlation coefficient,  $r$ , is calculated to estimate correlation between strength and density and G-modulus and density (Walpole, Myers, Myers & Ye, 2007). The results are shown in table 13.

**Table 13: Correlation between strength and density, G-modulus and density and G-modulus and strength**

	<b>Coefficient of correlation</b>
	<b><math>r</math></b>
<b>Between density and shear strength</b>	0,24
<b>Between density and G-modulus</b>	0,34

**Discussion**

The shear strengths calculated above seems to have a size-effect. This effect is recommended further investigated by performing more tests with different sizes for the shear area.

As seen from figures 44 and 45, and the coefficient of correlation,  $r$ , from table 13, there is no significant dependence of shear strength and G-modulus on density, which supports the idea that the shear strength is independent of glulam strength class.

The shear area used in this report is an estimate based on the computer models;  $A_{shear} = D * h$ . The real shear area might be measured after testing to see whether it corresponds to the estimated one. The surface of the shear area changes between tracing the annual rings tangential and “jumping” between rings radial as shown in figure 46. The total tangential area and the total radial area of the shear surface might be measured to obtain  $A_{radial}$  and  $A_{tangential}$  which may be used to investigate whether the shear strength and stiffness are different in radial and tangential direction.



**Figure 46: The shear area after fracture change between tracing the annual rings tangential and “jumping” from rings in radial direction.**



## **Conclusion and further work**

Results from part one has shown that the cuts of the specimen must overlap slightly in vertical direction in order for the specimen to form a shear plane at failure. Results from part two and part three has shown that there might be an influence of normal stress perpendicular to fibres, which means that the shear capacity probably is underestimated in this research. It is desired to eliminate the areas of tension in the specimen; hence, the specimen should be further optimized by varying the dimensions followed by testing in the laboratory before a conclusion can be drawn on how well the specimen is suited for shear testing.

The characteristic shear strength is estimated between 2.6 MPa and 3.6 MPa, which correspond well to values found in literature. The results indicate a decrease in shear strength by increasing specimen size, but further research is recommended in order to confirm the size-effect and to reveal the reason for it.

The value for the shear modulus estimated in this report is relatively high; approximately 970 MPa, which might be due to a simplified estimation method for the G-modulus. It is recommended that the elastic G-modulus is further investigated by means of a method similar to the one used by Dahl and Malo (2009a).



## References

- ASTM D143 (1984) Standard methods of testing small clear specimens of timber. American Society for Testing and Materials
- Dahl KB, Malo K. A. (2009a) Linear shear properties of spruce softwood. *Wood Sci Technol* (2009) 43:499–525 DOI 10.1007/s00226-009-0246-5
- Dahl K. B., Malo K. A. (2009b) Nonlinear shear properties of spruce softwood: experimental results. *Wood Sci Technol* (2009) 43:539–558. DOI 10.1007/s00226-009-0247-4
- Dahl K. B. (2009) Mechanical properties of clear wood from Norway spruce. ISBN 978-82-471-1911-2 (printed ver.) ISBN 978-82-471-1912-9 (electronic ver.) ISSN 1503-8181
- Daniel I. M., Ishai O. (2006). *Engineering mechanics of composite materials: Second edition*. Oxford University Press. ISBN 0-19-515097-X.
- Denzler J. K., Glos P. (2007) Determination of shear strength values according to EN 408. *Holzforschung München, Technische Universität München, Germany*. DOI 10.1617/s11527-006-9199-4
- Klapp H, Brüninghoff H (Presented to CIB/W18(A) in August 2005) Shear strength of glued laminated timber. *Bergische Universität Wuppertal, Germany*.
- NS-EN 338 (2003) Structural timber strength classes. European Committee for Standardization, 2<sup>nd</sup> edn
- NS-EN 384 (2004) Structural timber—determination of characteristic values of mechanical properties and density. European Committee for Standardization
- NS-EN 408 (2003) Timber structures—structural timber and glued laminated timber. Determination of some physical and mechanical properties. European Committee for Standardization (2nd ed.)
- NS-EN 1194 (1999) Timber Structures - Glued laminated timber - Strength classes and determination of characteristic values. European Committee for Standardization
- NS-EN 14358 (2006) Timber Structures – Calculation of characteristic 5-percentile values and acceptance criteria for a sample. European Committee for Standardization
- Schickhofer G (Presented to CIB/W18(A) in August 2001) Determination of shear strength values for GLT using visual and machine graded spruce laminations. *Graz University of Technology, Institute for Steel, Timber and Shell Structures*.
- SKOGFORSK (1992) Skandinaviske normer for testing av små feilfrie prøver av heltre, SKANORM. Dept. of Forestry, Agricultural University of Norway

Walpole R. E., Myers R. H., Myers S. L. Ye K. (2007) Probability & Statistics for Engineers & Scientists: Eight edition. Pearson Education International. ISBN 0-13-204767-5.

Om Limtre. Read 07.06.2012 from <http://www.moelven.com/Produkter-og-tjenester/Limtre/Bygge-med-Limtre/Hvorfor-bruke-Limtre/>

## Appendix A: Transformation from engineering constants to stiffness parameters, C

Equations from Daniel and Ishai (2006) are used in the following.

**Table 14 Linear elastic stiffness properties of Norway spruce with density 400 kg/m<sup>3</sup>.**

Symbol	$E_{LL}$	$E_{RR}$	$E_{TT}$	$\nu_{LR}$	$\nu_{LT}$	$\nu_{RT}$	$G_{LR}$	$G_{LT}$	$G_{TR}$
Value	10000 MPa	800 MPa	400 MPa	0.5	0.6	0.6	600 MPa	600 MPa	30 MPa

The elastic engineering constants are transformed into stiffness parameters which are needed in order to model an orthotropic material in ABAQUS. The stiffness parameters relate stresses to strains by

$$[\sigma] = [C][\varepsilon]$$

The stiffness matrix [C] containing stiffness parameters is given by

$$[C] = \begin{bmatrix} C_{11} & C_{12} & C_{13} & 0 & 0 & 0 \\ C_{21} & C_{22} & C_{23} & 0 & 0 & 0 \\ C_{31} & C_{32} & C_{33} & 0 & 0 & 0 \\ 0 & 0 & 0 & C_{44} & 0 & 0 \\ 0 & 0 & 0 & 0 & C_{55} & 0 \\ 0 & 0 & 0 & 0 & 0 & C_{66} \end{bmatrix}$$

Where indexes 1, 2, 3, 4, 5 and 6 indicate principal axes and depend on the orientation of the fibres. Stiffnesses  $C_{ij}$  is related to engineering constants by

$$C_{11} = \frac{1 - \nu_{23}\nu_{32}}{E_2 E_3 \Delta}$$

$$C_{22} = \frac{1 - \nu_{13}\nu_{31}}{E_1 E_3 \Delta}$$

$$C_{33} = \frac{1 - \nu_{12}\nu_{21}}{E_1 E_2 \Delta}$$

$$C_{12} = \frac{\nu_{21} + \nu_{31}\nu_{23}}{E_2 E_3 \Delta} = \frac{\nu_{12} + \nu_{13}\nu_{32}}{E_1 E_3 \Delta}$$

$$C_{23} = \frac{\nu_{32} + \nu_{12}\nu_{31}}{E_1 E_3 \Delta} = \frac{\nu_{23} + \nu_{21}\nu_{13}}{E_1 E_2 \Delta}$$

$$C_{11} = \frac{v_{13} + v_{12}v_{23}}{E_1E_2\Delta} = \frac{v_{31} + v_{21}v_{32}}{E_2E_3\Delta}$$

$$C_{44} = C_{23}$$

$$C_{55} = C_{13}$$

$$C_{66} = C_{12}$$

Where

$$\Delta = \frac{1}{E_1E_2E_3} \begin{vmatrix} 1 & -v_{21} & -v_{31} \\ -v_{12} & 1 & -v_{32} \\ -v_{13} & -v_{23} & 1 \end{vmatrix}$$

The calculation of the stiffness parameters is done using the following code from MATLAB:

```
clear all
clc

% R=1, T=2, L=3 for coordinates in ABAQUS

ELL=10000; %E33
ERR=800; %E11
ETT=400; %E22
vLR=0.5; %v31
vLT=0.6; %v32
vRT=0.6; %v12
GLR=600; %G31
GLT=600; %G32
GTR=30; %G21

vTL=ETT*vLT/ELL; %v23
vRL=ERR*vLR/ELL; %v13
vTR=ETT*vRT/ERR; %v21

Delta=[1 -vTR -vLR; -vRT 1 -vLT; -vRL -vTL 1];
d=1/(ELL*ERR*ETT)*det(Delta);

CLL=(1-vRT*vTR)/(ERR*ETT*d); %C33
CRR=(1-vTL*vLT)/(ELL*ETT*d); %C11
CTT=(1-vLR*vRL)/(ELL*ERR*d); %C22
CLR=(vRL+vRT*vTL)/(ERR*ETT*d); CRL=CLR; %C31 C13
CRT=(vTR+vLR*vTL)/(ELL*ETT*d); CTR=CRT; %C12 C21
CLT=(vLT+vRT*vLR)/(ELL*ERR*d); CTL=CLT; %C32 C23
C44=GLT; %G32
C55=GLR; %G31
C66=GTR; %G21

C=[CRR CRT CRL 0 0 0;
   CTR CTT CTL 0 0 0;
   CLR CLT CLL 0 0 0;
   0 0 0 C44 0 0;
   0 0 0 0 C55 0;
   0 0 0 0 0 C66;]

% C=[C1111 C1122 C1133 0 0 0;
```

```

% C2211 C2222 C2233 0 0 0;
% C3311 C3322 C3333 0 0 0;
% 0 0 0 C2323 0 0;
% 0 0 0 0 C1313 0;
% 0 0 0 0 0 C1212;];

```

The result is

C =

1.0e+004 \*

```

0.1022 0.0324 0.0705 0 0 0
0.0324 0.0508 0.0467 0 0 0
0.0705 0.0467 1.0633 0 0 0
0 0 0 0.0600 0 0
0 0 0 0 0.0600 0
0 0 0 0 0 0.0030

```

**Table 15: Values from MATLAB**

C1111 = CRRRR	1022
C1122 = CRRTT	324
C2222 = CTTTT	508
C1133 = CRLL	705
C2233 = CTLL	467
C3333 = CLLLL	10633
C1212 = CRTRT	30
C1313 = CRLRL	600
C2323 = CTLTL	600



# Appendix B: Results on time, extension and applied force from test machine INSTRON

The results from the test machine are plotted for all specimens as shown below.

## Part one

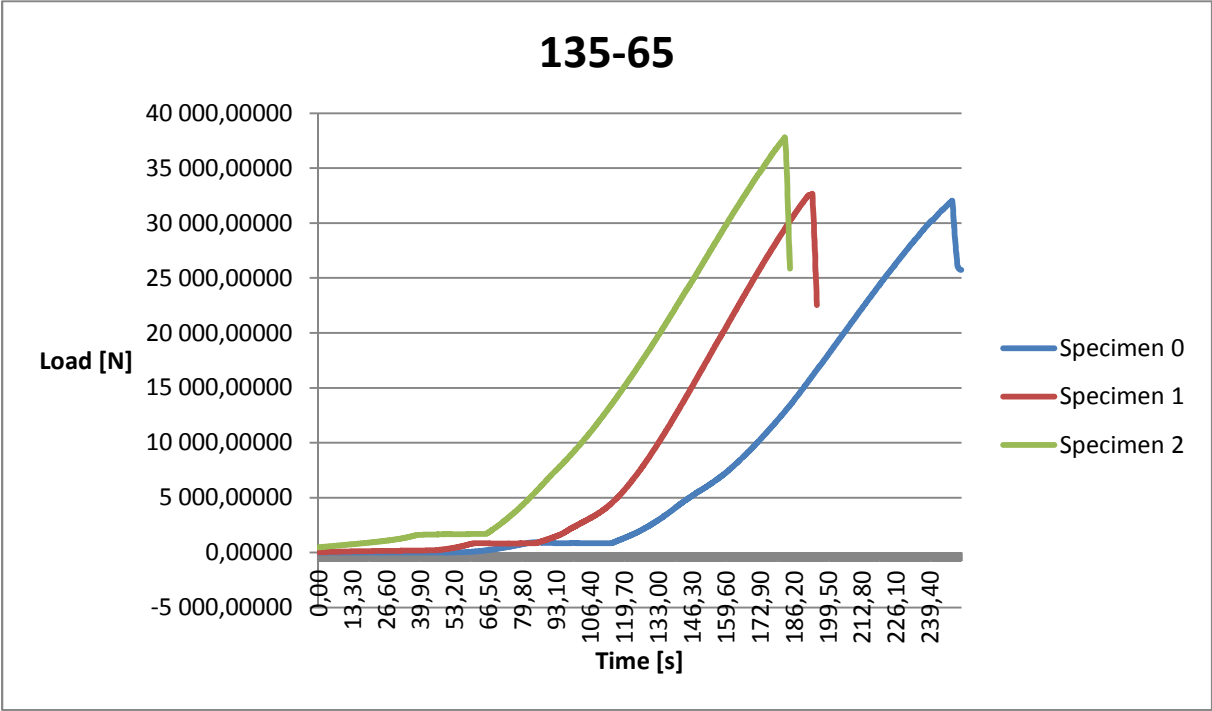


Figure 47: Load (N) versus time (s) plotted for specimen 135-65 from part one

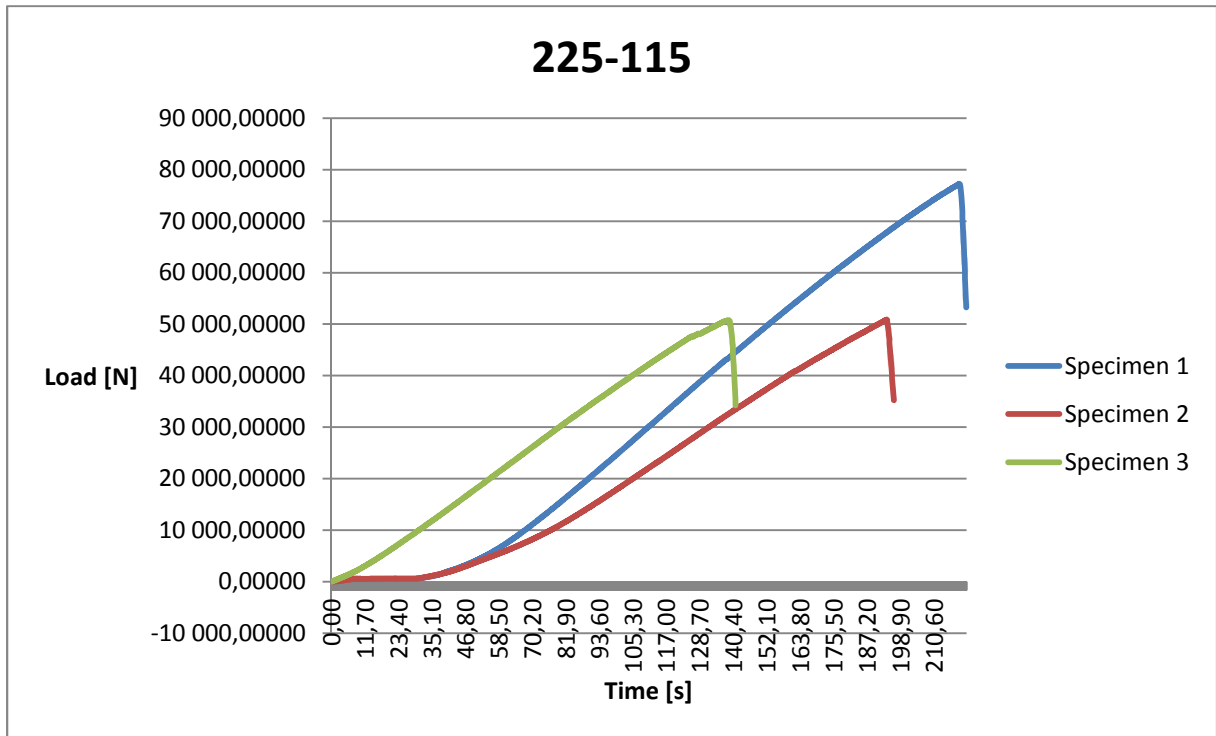


Figure 48: Load (N) versus time (s) plotted for specimen 225-115 from part one

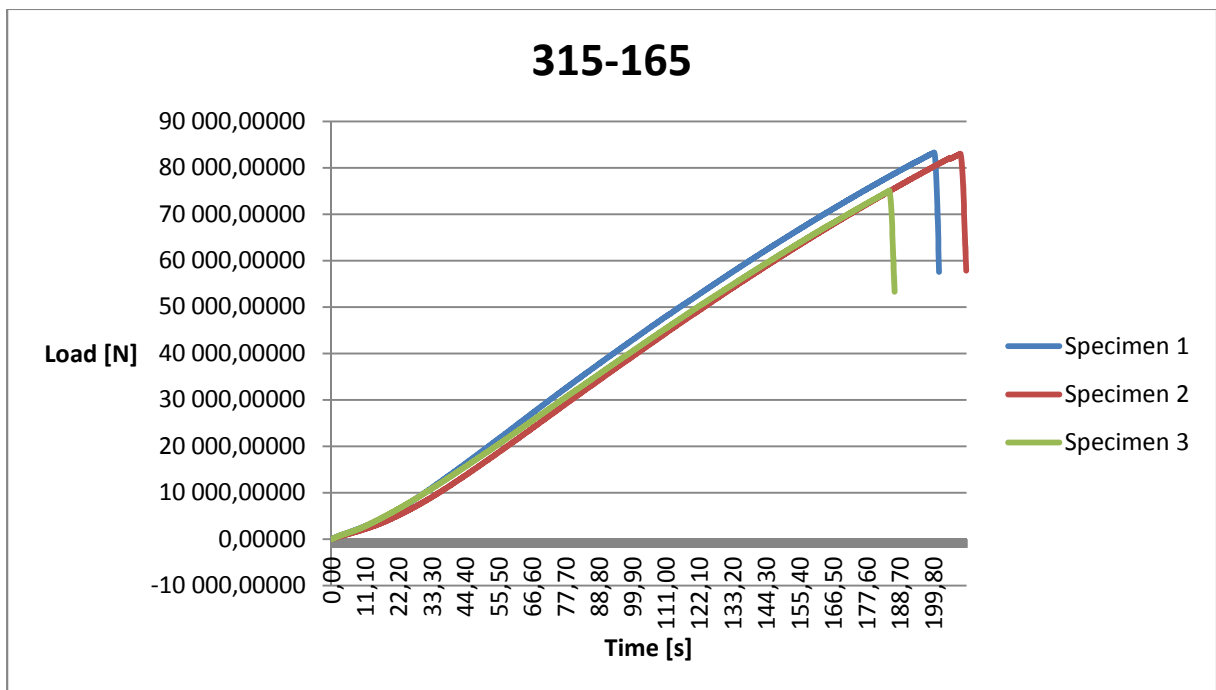


Figure 49: Load (N) versus time (s) plotted for specimen 315-165 from part one

Part two

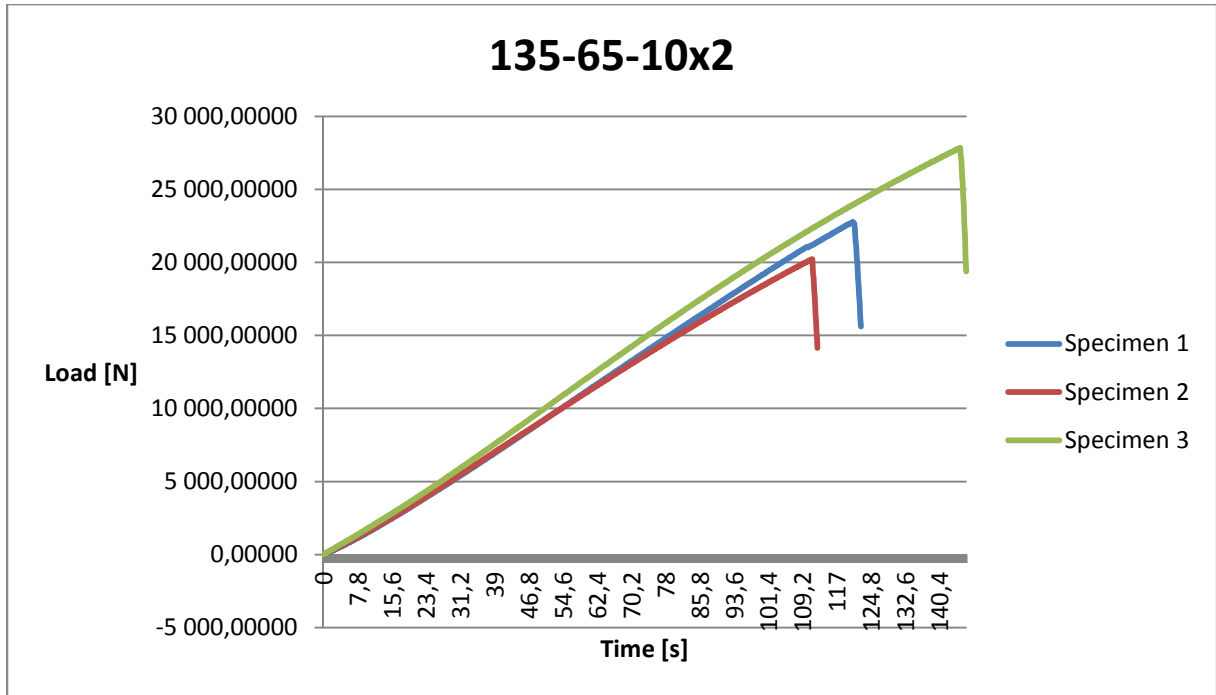


Figure 50: Load (N) versus time (s) plotted for specimen 135-65-10x2 from part two

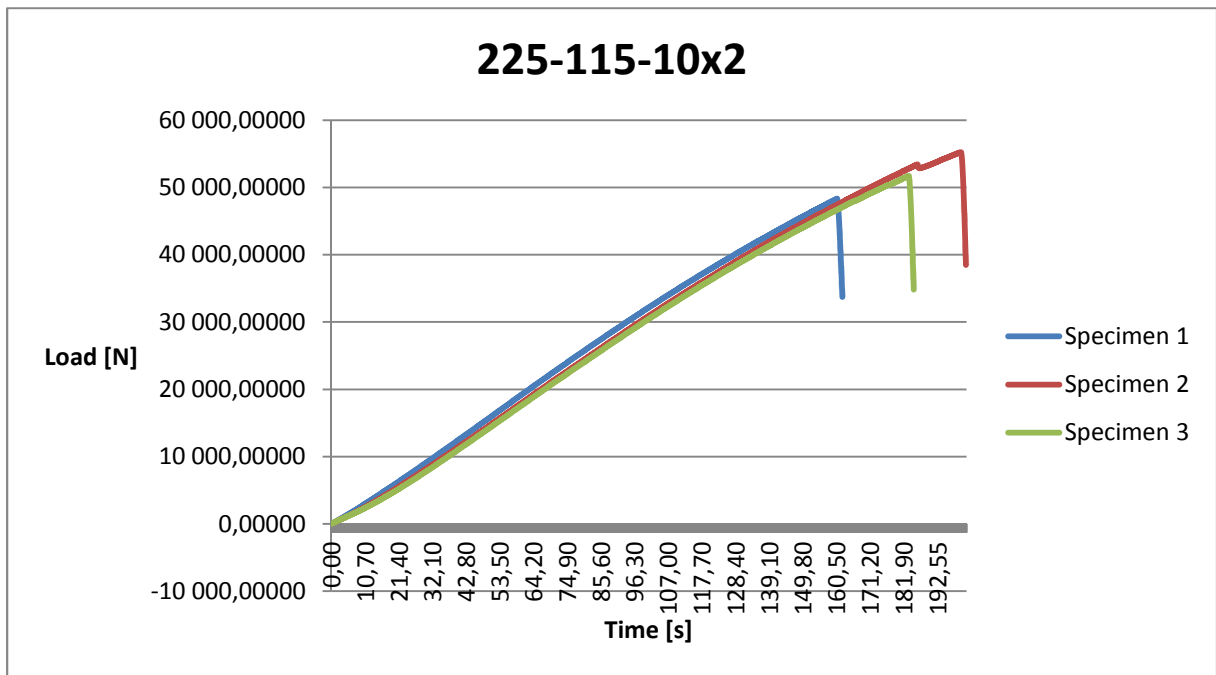


Figure 51: Load (N) versus time (s) plotted for specimen 225-115-10x2 from part two

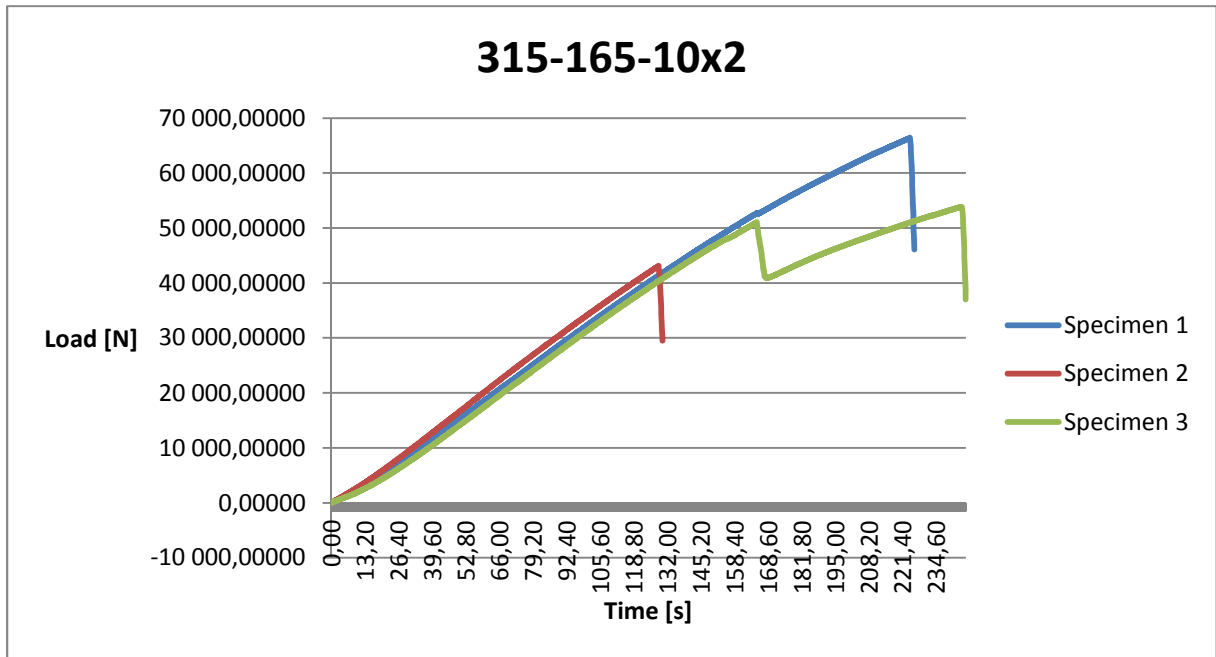


Figure 52: Load (N) versus time (s) plotted for specimen 315-165-10x2 from part two

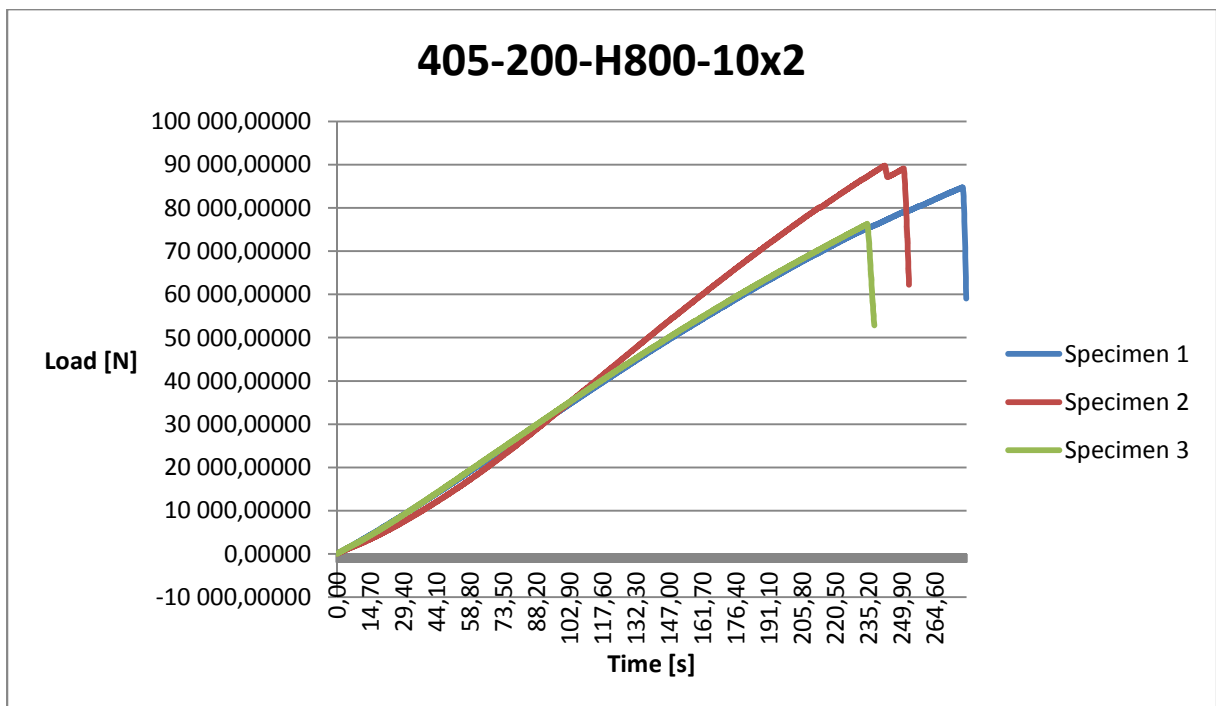
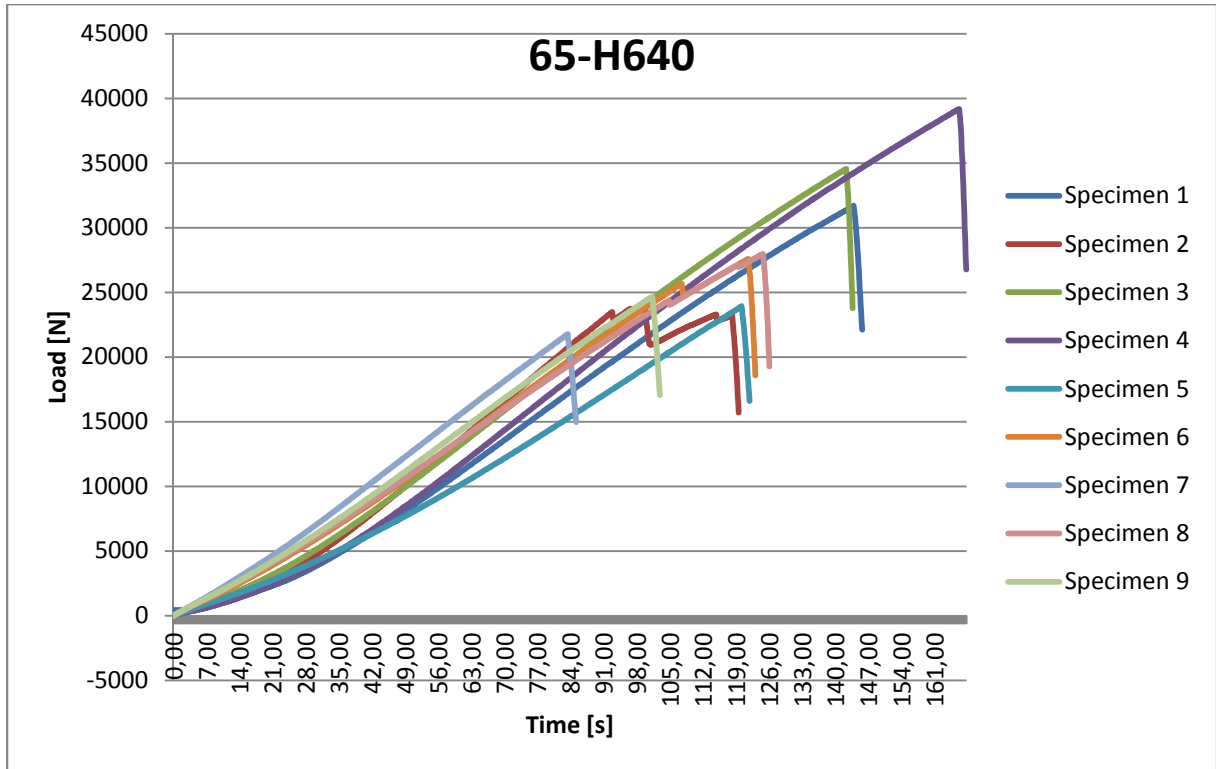
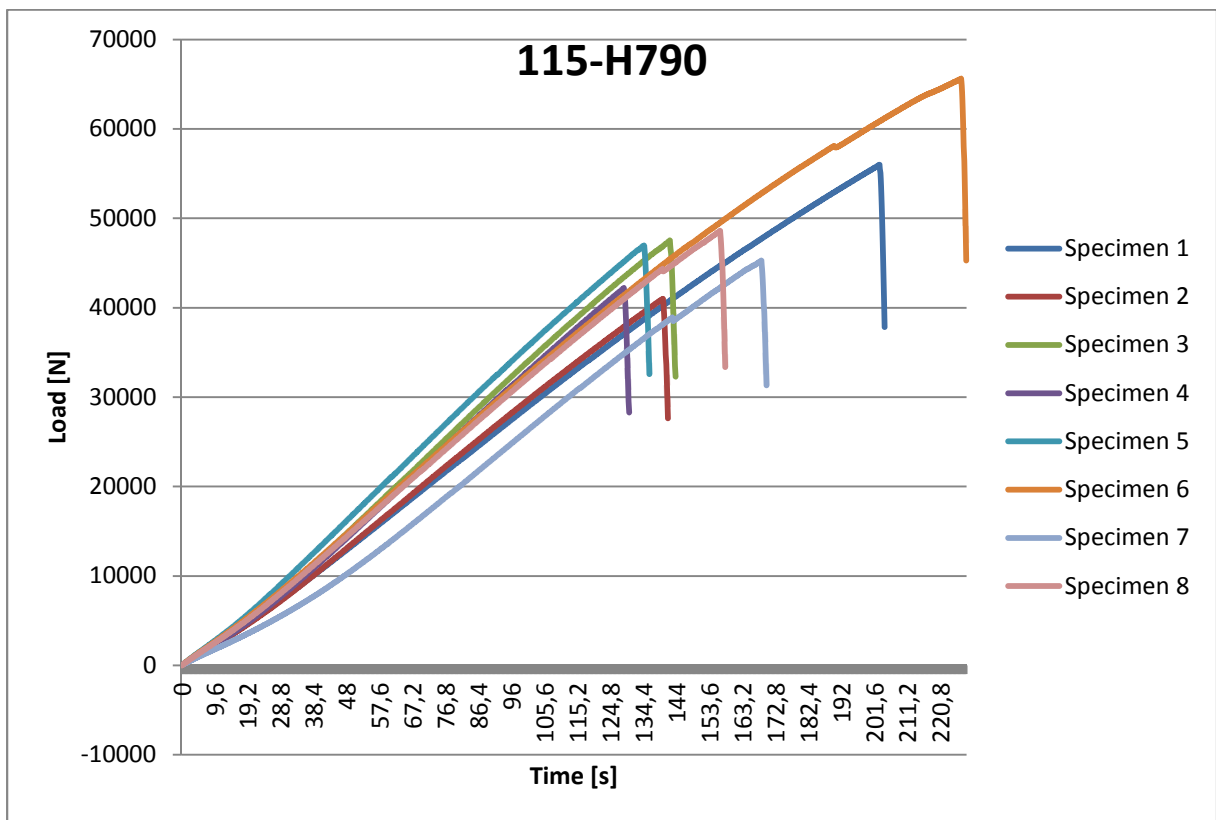


Figure 53: Load (N) versus time (s) plotted for specimen 405-200-H800-10x2 from part two

**Part three**



**Figure 54: Load (N) versus time (s) plotted for specimen 65-H640 from part three**



**Figure 55: Load (N) versus time (s) plotted for specimen 115-H790 from part three**

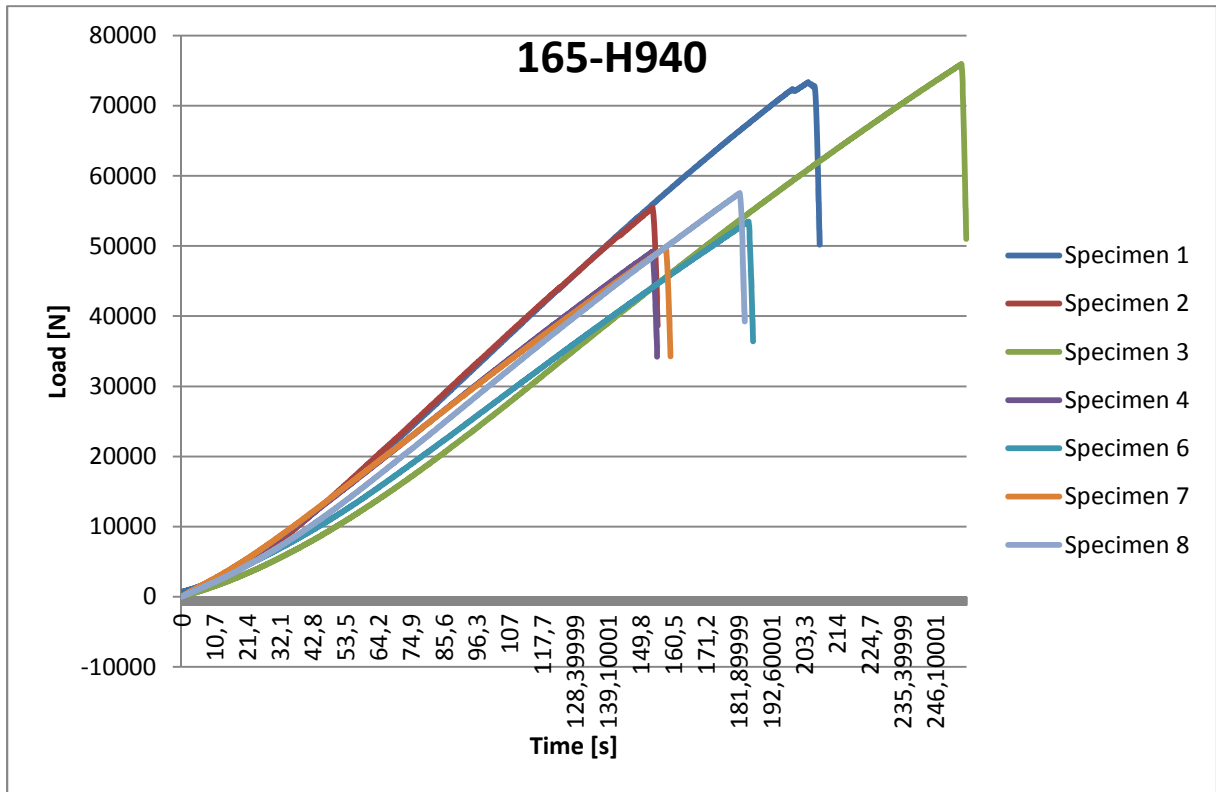


Figure 56: Load (N) versus time (s) plotted for specimen 165-H940 from part three

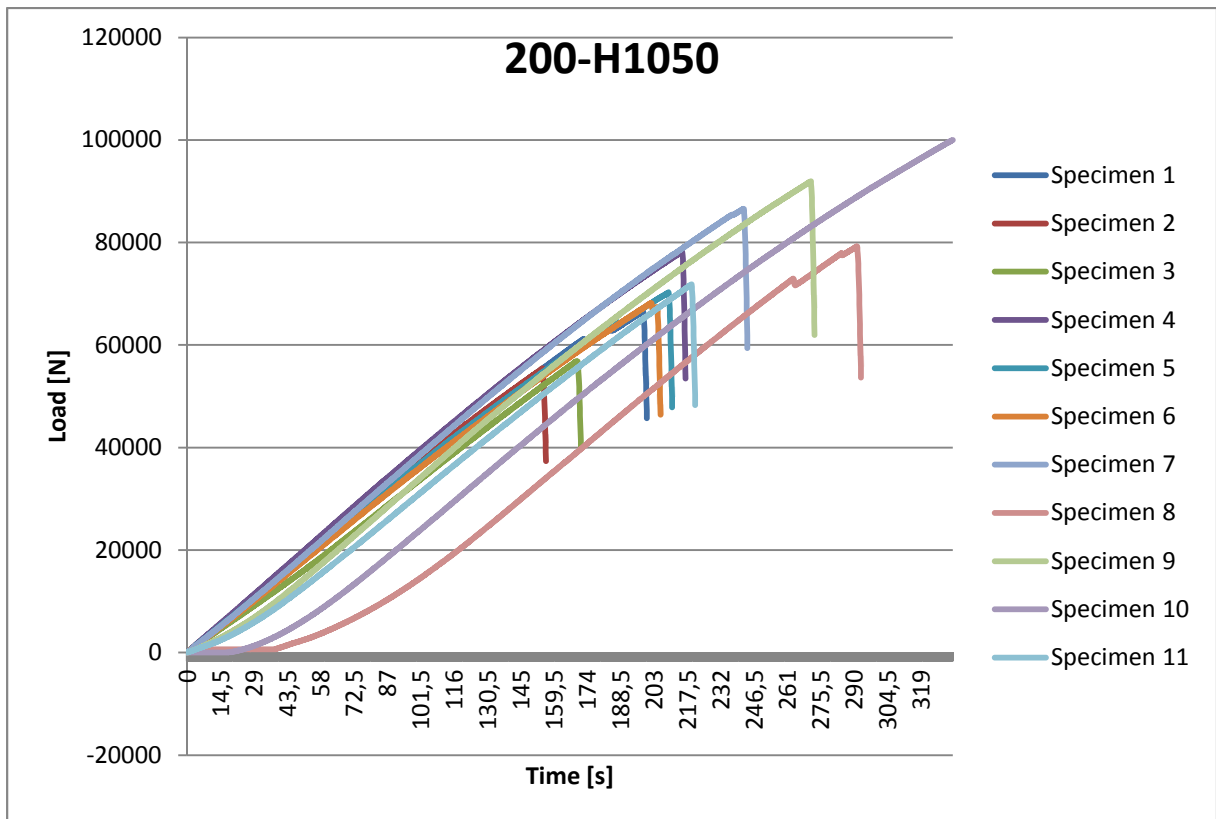


Figure 57: Load (N) versus time (s) plotted for specimen 200-H1050 from part three

# Appendix C: Pictures of specimens after failure

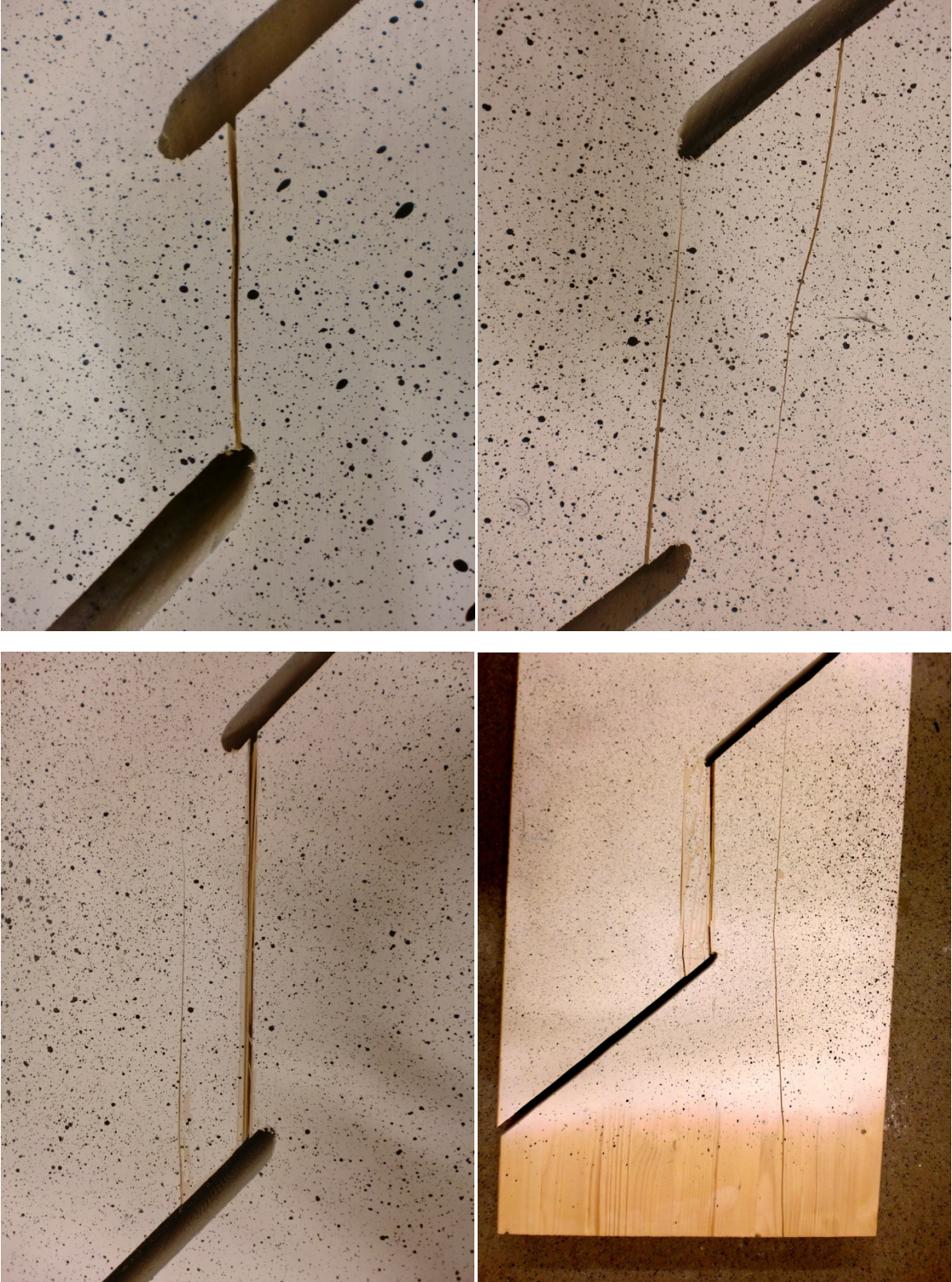
## Part one

The specimens from part one formed typical cracks as shown below.



**Part two**

The specimens from part two formed typical cracks as shown below.





**Part three**

The specimens from part three formed typical cracks as shown below.



**Appendix D: Calculations concerning shear strength from INSTRON test machine and G-modulus from ARAMIS (video extensometry)**

**PART ONE**

**Table 16: Calculations on shear strength from part one**

<b>SPECIMEN NO.</b>	<b>AREA OF SHEARPLANE (mm<sup>2</sup>)</b>	<b>MAX LOAD (FAILURE) (N)</b>	<b>estimated CAPACITY (mi)</b>	<b>MIDDLE estimatedCAPACITY</b>	<b>standard dev. (mi)</b>	<b>COV</b>	<b>ks(n=3)</b>	<b>mk=characteristic capacity=f(05)</b>
	(h*D)							
<b>135-65-0 (1a-0)</b>	5850	32041,84618	5,477					
<b>135-65-1 (1a-1)</b>	5850	32663,71094	5,584	<b>5,841</b>	0,540	0,092	3,15	<b>4,38208944</b>
<b>135-65-2 (1a-2)</b>	5850	37796,77344	6,461					
<b>225-115-1 (2b-1)</b>	10350	77245,21094	7,463					
<b>225-115-2 (2b-2)</b>	10350	50890,42969	4,917	<b>5,762</b>	1,474	0,256	3,15	<b>2,6371813</b>
<b>225-115-3 (2b-3)</b>	10350	50762,47266	4,905					
<b>315-165-1 (3c-1)</b>	14850	83291,28906	5,609					
<b>315-165-2 (3c-2)</b>	14850	83036,46094	5,592	<b>5,418</b>	0,315	0,058	3,15	<b>4,62331138</b>
<b>315-165-3 (3c-3)</b>	14850	75054,11719	5,054					

## PART TWO

**Table 17: Calculations on shear strength from part two**

SPECIMEN NO.	AREA OF SHEARPLANE (mm <sup>2</sup> )	MAX LOAD (FAILURE) (N)	comments	CAPACITY (Mpa)	MIDDLE CAPACITY (Mpa)	n = NO. OF TESTS	st. dev(mi)	COV=s/m(mean)	ks	mk=f(05)
	(h*D)		SP = shear plane(s)							
135-65-10x2-1	5850	22 764,72656	2 SP, nice graph	3,891						
135-65-10x2-2	5850	20 229,95312	1 SP, split, nice graph	3,458	<b>4,036</b>	3	0,6628795	0,16422	3,15	<b>2,40532626</b>
135-65-10x2-3	5850	27 845,11523	1 SP, split, nice graph	4,760						
225-115-10x2-1	10350	48 341,51953	2 SP, nice graph	4,671						
225-115-10x2-2	10350	55 241,91797	1 SP, split (tendency to 2 SP), nice graph (one small peak at ~ 53 kN)	5,337	<b>5,002</b>	3	1,2285270	0,24561	3,15	<b>2,06956572</b>
225-115-10x2-3	10350	51 725,73828	1 SP, split (tendency to 2 SP), nice graph	4,998						
315-165-10x2-1	14850	66 398,12500	2 SP, knot, nice graph	4,471						
315-165-10x2-2	14850	43 109,91016	1 SP, split, (tendency to 2 SP), nice graph	2,903	<b>3,667</b>	3	0,9057562	0,24698	3,15	<b>1,64367742</b>
315-165-10x2-3	14850	53 871,50000	1 SP, split, best shear surface!, bad graph:	3,628						

			two peaks: first peak due to crack in top. Last failure used in calc.							
405-200-H800-10x2-1	18000	84 707,80469	1 SP, split, (tendency to 2 SP), nice graph, cracks in top!	4,706						
405-200-H800-10x2-2	18000	89 767,57031	2 SP, two peaks on graph (due to crack in top?), load at first failure used in calc.	4,987	<b>4,847</b>	2	1,1627449	0,23991	3,15	<b>2,04626750</b>
405-200-H800-10x2-3	18000	76 280,58594	FAILURE DUE TO CRACKS IN TOP/BOTTOM	4,238						

**Table 18: Calculations on stiffness from part two**

SPECIMEN NO.	TauXY at 0.2Fmax	mean EXY 0.2Fmax	TauXY at 0.5Fmax	mean EXY 0.5Fmax	TauXY at 0.8Fmax	mean EXY 0.8 Fmax	G (0.2-0.5)	G(0.5-0.8)	G(0.2-0.8)	<i>G modulus</i>	<i>MIDDLE G MODULUS</i>
135-65-10x2-1	0,84	8,45E-04	1,92	2,19E-03	3,11	3,87E-03	805,30	708,98	751,75	<b>755,34</b>	
135-65-10x2-2	0,73	1,26E-03	1,79	2,23E-03	2,72	3,52E-03	1 092,32	721,08	881,05	<b>898,15</b>	<b>873,66</b>
135-65-10x2-3	1,04	6,24E-04	2,41	2,20E-03	3,78	3,48E-03	869,01	1 073,06	960,37	<b>967,48</b>	
225-115-10x2-1	1,01	9,96E-04	2,32	2,01E-03	3,69	3,18E-03	1 289,90	1 173,97	1 227,93	<b>1 230,60</b>	
225-115-10x2-2	1,07	7,91E-04	2,71	2,54E-03	4,26	4,27E-03	935,16	898,82	917,16	<b>917,05</b>	<b>1 072,05</b>
225-115-10x2-3	1,00	6,82E-04	2,46	2,31E-03	3,94	3,48E-03	895,24	1 261,70	1 048,57	<b>1 068,50</b>	
315-165-10x2-1	0,92	1,01E-03	2,24	2,18E-03	3,61	3,42E-03	1 133,59	1 099,31	1 115,96	<b>1 116,29</b>	
315-165-10x2-2	0,59	1,01E-04	1,43	1,32E-03	2,32	2,25E-03	693,29	954,95	806,12	<b>818,12</b>	<b>916,45</b>
315-165-10x2-3	0,79	1,06E-03	1,81	2,40E-03	2,89	3,64E-03	755,49	876,08	813,26	<b>814,95</b>	
405-200-H800-10x2-1	0,98	1,09E-03	2,35	2,51E-03	3,73	4,34E-03	966,01	754,93	846,92	<b>855,95</b>	
405-200-H800-10x2-2	1,04	7,94E-04	2,47	1,88E-03	3,95	3,12E-03	1 320,27	1 189,79	1 250,47	<b>1 253,51</b>	<b>1 069,64</b>
405-200-H800-10x2-3	0,89	1,03E-03	2,12	0,00	3,35	0,00	956,15	1 255,66	1 086,52	<b>1 099,44</b>	

### PART THREE

**Table 19: Calculations on shear strength from part three**

SPECIMEN NO.	AREA OF SHEARPLANE (mm <sup>2</sup> )	MAX LOAD (FAILURE) (N)	comments	CAPACITY (Mpa)	MEAN CAPACITY (mi(mean))(Mpa)	n = NO. OF TESTS	st. dev.(mi)	COV	ks	mk=f(05)
	(h*D)									lin. Interpolation
65-H640-1	5850	31 686,72	2 SP, nice graph Inst.	5,417						
65-H640-2	5850	24 054,91	2 SP? (didnt split due to knot), bad graph, calculations at "first" failure (highest load)	4,112						
65-H640-3	5850	34 547,58	1 SP, split (tendency to 2 SP), nice graph Ins.	5,906						
65-H640-4	5850	39 182,22	1 SP, split, (tendency to 2 SP), nice graph	6,698						
65-H640-5	5850	23 918,50	2 SP, nice graph Inst.	4,089	<b>4,850</b>	9	0,98	0,20	2,17	<b>3,13</b>
65-H640-6	5850	27 586,18	1 SP, didnt split, two peaks on graph, calculations on last failure	4,716						
65-H640-7	5850	21 766,67	2 SP, nice graph Inst.	3,721						
65-H640-8	5850	27 970,40	2 SP, bad graph Inst. (three failure points), last failure point used in calc.	4,781						
65-H640-9	5850	24 646,41	2 SP, nice graph Inst.	4,213						

115-H790-1	10350	55 988,03	1 SP, split, (tendency to 2 SP), nice graph	5,409							
115-H790-2	10350	40 989,90	1 SP, split, (tendency to 2 SP), nice graph	3,960							
115-H790-3	10350	47 526,58	2 SP, nice graph	4,592							
115-H790-4	10350	42 210,46	1 SP, split, (tendency to 2 SP), nice graph	4,078	<b>4,748</b>	8	0,78	0,16	2,24	<b>3,33</b>	
115-H790-5	10350	46 962,83	2 SP, nice graph	4,537							
115-H790-6	10350	65 601,74	1 SP, split, (tendency to 2 SP), nice graph (one small crack at ~ 58 kN)	6,338							
115-H790-7	10350	45 272,20	2 SP (knot?), nice graph (one small crack at ~ 39 kN)	4,374							
115-H790-8	10350	48 600,36	1 SP, split, (tendency to 2 SP), nice graph (one small crack at ~ 45 kN)	4,696							
165-H940-1	14850	73 345,01	1 SP, split (tendency to 2 SP), nice graph ("round failure")	4,939							
165-H940-2	14850	55 465,45	2 SP, nice graph	3,735							
165-H940-3	14850	75 916,78	1 SP, split (tendency to 2 SP), nice graph	5,112							
165-H940-4	14850	49 190,76	2 SP, nice graph	3,313	<b>3,990</b>	7	0,74	0,18	2,32	<b>2,62</b>	
165-H940-5	14850	N.A.	BROKEN								
165-H940-6	14850	53 488,74	1 SP, split (tendency to 2 SP), nice graph	3,602							

165-H940-7	14850	49 816,20	1 SP, split (tendency to 2 SP), nice graph	3,355							
165-H940-8	14850	57 526,07	2 SP, nice graph	3,874							
200-H1050-1	18000	66 565,91	2 SP, bad graph Inst. (three failure points), last failure point used in calc.	3,698							
200-H1050-2	18000	55 443,32	1 SP, split (tendency to 2 SP), nice graph	3,080							
200-H1050-3	18000	56 797,75	2 SP, nice graph	3,155							
200-H1050-4	18000	78 251,35	1 SP, split (tendency to 2 SP), nice graph	4,347							
200-H1050-5	18000	70 256,33	2 SP (knot?), nice graph (one small crack at ~ 65 kN)	3,903							
200-H1050-6	18000	68 228,95	2 SP, two peaks at failure, calculations done at first failure	3,790	<b>4,029</b>	10	0,65	0,16	2,10	<b>2,82</b>	
200-H1050-7	18000	86 596,13	2 SP, nice graph	4,811							
200-H1050-8	18000	79 270,33	2 SP, bad graph Inst. (three failure points), last failure point used in calc.	4,404							
200-H1050-9	18000	91 943,43	1 SP, split (tendency to 2 SP), nice graph	5,108							
200-H1050-10	18000	over 100 000	no failure, no sign of shear planes or cracks								
200-H1050-11	18000	71 838,59	1 SP, split (tendency to 2 SP), nice graph	3,991							

**Table 20: Calculations on stiffness from part three**

SPECIMEN NO.	TauXY at 0.2Fmax	mean EXY 0.2Fmax	TauXY at 0.5Fmax	mean EXY 0.5Fmax	TauXY at 0.8Fmax	mean EXY 0.8 Fmax	G (0.2-0.5)	G(0.5-0.8)	G(0.2-0.8)	<b>G modulus</b>	<b>MIDDLE G modulus</b>
65-H640-1		no data		no data		no data					
65-H640-2	0,91	1,53E-03	2,07	3,00E-03	3,17	3,47E-03	786,59	2 348,56	1 164,54	<b>1 433,23</b>	
65-H640-3	1,27	6,18E-04	2,94	2,52E-03	4,68	4,24E-03	874,76	1 013,20	940,39	<b>942,79</b>	
65-H640-4	1,45	8,86E-04	3,29	2,42E-03	5,31	4,49E-03	1 199,49	974,57	1 070,17	<b>1 081,41</b>	
65-H640-5		no data		no data		no data					
65-H640-6	0,86	1,13E-03	2,34	2,92E-03	3,64	4,06E-03	822,72	1 141,07	945,96	<b>969,92</b>	<b>1 174,36</b>
65-H640-7	0,80	2,38E-04	1,87	1,29E-03	2,84	1,95E-03	1 020,39	1 465,67	1 191,88	<b>1 225,98</b>	
65-H640-8	1,02	1,22E-03	2,37	1,81E-03	3,72	3,05E-03	2 310,53	1 078,73	1 470,78	<b>1 620,01</b>	
65-H640-9	0,93	7,86E-04	2,08	2,04E-03	3,27	3,25E-03	912,35	982,30	946,84	<b>947,16</b>	
115-H790-1	1,15	7,26E-04	2,69	1,87E-03	4,30	3,57E-03	1 350,83	941,79	1 106,29	<b>1 132,97</b>	
115-H790-2	0,80	6,22E-04	1,96	1,94E-03	3,09	3,14E-03	878,96	942,66	909,31	<b>910,31</b>	
115-H790-3	0,94	6,91E-04	2,27	2,01E-03	3,59	3,28E-03	1 005,64	1 045,77	1 025,25	<b>1 025,55</b>	

115-H790-4	0,87	6,74E-04	2,07	1,81E-03	3,17	2,77E-03	1 053,58	1 149,00	1 097,28	<b>1 099,95</b>	
115-H790-5	0,93	7,04E-04	2,30	2,06E-03	3,56	3,03E-03	1 008,70	1 300,52	1 129,74	<b>1 146,32</b>	<b>1 057,57</b>
115-H790-6	1,30	1,01E-03	3,14	2,61E-03	5,02	4,44E-03	1 146,84	1 021,73	1 080,03	<b>1 082,87</b>	
115-H790-7	0,89	1,04E-03	2,17	2,17E-03	3,49	3,48E-03	1 133,47	1 010,89	1 067,70	<b>1 070,69</b>	
115-H790-8	1,00	9,38E-04	2,35	2,36E-03	3,75	3,71E-03	947,37	1 037,12	991,09	<b>991,86</b>	
165-H940-1	1,06	7,09E-04	2,47	no data	3,94	2,20E-03	no data	no data	1 924,53	<b>1 924,53</b>	
165-H940-2	0,77	6,22E-04	1,85	1,94E-03	2,95	3,14E-03	824,97	911,83	866,35	<b>867,72</b>	
165-H940-3	1,05	1,08E-03	2,56	2,61E-03	4,08	4,00E-03	987,70	1 089,14	1 035,99	<b>1 037,61</b>	
165-H940-4	0,70	3,79E-04	1,63	1,39E-03	2,63	2,41E-03	916,56	984,90	950,84	<b>950,77</b>	<b>1 125,19</b>
165-H940-5	0,00	broken	0,00	broken	0,00	broken					
165-H940-6	0,74	4,84E-04	1,77	1,38E-03	2,84	2,37E-03	1 145,29	1 086,05	1 114,37	<b>1 115,24</b>	
165-H940-7	0,71	4,12E-04	1,70	1,55E-03	2,67	2,50E-03	868,19	1 018,21	936,52	<b>940,97</b>	
165-H940-8	0,79	6,31E-04	1,94	1,74E-03	3,04	2,79E-03	1 041,00	1 037,99	1 039,53	<b>1 039,51</b>	
200-H1050-1	0,79	3,51E-02	1,86	1,28E-01	2,92	2,06E-01	11,44	13,67	12,46	<b>12,52</b>	

200-H1050-2	0,62	2,11E-04	1,52	1,12E-03	2,44	2,20E-03	994,09	847,01	914,37	<b>918,49</b>	
200-H1050-3	0,66	8,91E-05	1,60	1,21E-03	2,51	2,05E-03	838,73	1 076,03	940,60	<b>951,79</b>	
200-H1050-4	0,89	6,75E-04	2,15	1,72E-03	3,44	2,40E-03	1 213,02	1 896,52	1 483,05	<b>1 530,86</b>	
200-H1050-5	0,80	5,34E-04	1,99	1,56E-03	3,07	2,37E-03	1 157,23	1 348,05	1 241,25	<b>1 248,84</b>	<b>1 242,40</b>
200-H1050-6	0,78	7,41E-04	1,90	1,86E-03	2,99	2,85E-03	1 003,83	1 098,42	1 048,42	<b>1 050,22</b>	
200-H1050-7	0,99	3,79E-04	2,44	1,55E-03	3,80	1,91E-03	1 241,55	3 809,19	1 841,24	<b>2 297,33</b>	
200-H1050-8	0,92	8,53E-04	2,18	1,87E-03	3,51	2,89E-03	1 232,76	1 306,51	1 269,59	<b>1 269,62</b>	
200-H1050-9	1,08	8,74E-04	2,55	2,53E-03	4,05	4,19E-03	892,91	903,11	898,02	<b>898,01</b>	
200-H1050-10	1,13	1,15E-03	2,80	2,68E-03	4,45	4,69E-03	1 090,95	821,31	937,39	<b>949,88</b>	
200-H1050-11	0,85	6,69E-04	1,96	1,50E-03	3,15	2,43E-03	1 336,44	1 282,44	1 308,01	<b>1 308,96</b>	